Kinematical analysis of heavy-ion induced nuclear reactions using solid-state nuclear track detectors: A review

P. A. Gottschalk,[1)] P. Vater, and R. Brandt
Kernchemie, FB 14, Philipps-Universität, D-35032 Marburg, Germany

I. E. Qureshi and H. A. Khan
Radiation Physics Division, PINSTECH, P.O. Nilore, Islamabad, Pakistan

G. Fiedler
II. Physikalisches Institut, Justus-Liebig-Universität, D-35392 Giessen, Germany

Fiz. Élem. Chastits At. Yadra **27**, 377–430 (March–April 1996)

In reactions of heavy ions with heavy target nuclei, different multiplicities of heavy fragments are observed in the exit channel. These multiplicities have been found to vary between 2 and 5 in the present work. The heavy reaction fragments can be recorded in Solid State Nuclear Track Detectors (SSNTD) in the form of latent damage trails which can be etched and studied using an optical microscope. Each nuclear interaction can be investigated individually by measuring geometrical parameters of the correlated tracks. On the basis of the method of kinematical analysis first introduced in 1979, one can quantitatively determine the properties characterizing a nuclear reaction such as masses, energies, angles, and other parameters. This method allowed the first exclusive investigation of heavy-ion induced nuclear interactions with high multiplicities. The bulk of the reactions have been found as being due to sequential or multiple sequential fission. The reaction cross sections have been measured directly as well as derived from the elastic scattering data using semiquantal models. The present report describes and reviews results using SSNTDs in the study of heavy-ion reactions and the analysis of data performed by the method of kinematical analysis. New and unpublished results are also presented. [S1063-7796(96)00302-6]

1. INTRODUCTION

The history of using insulating materials as particle detectors can be traced back to the late 50s. In 1958, Young[1] set the stage for the introduction of a new and versatile detection system, by optically observing the fission-fragment tracks in LiF after chemical etching of the crystal. In the succeeding year, Silk and Barnes[2] reported that the radiation damage caused by fission fragments in mica is directly observable as thin long tracks when viewed through a transmission electron microscope. The enlargement of these tracks by chemical etching in the case of mica was discovered by Price and Walker,[3] who were unaware of the similar work done by Young. During the 60s, the team of Fleischer, Price, and Walker[4] greatly extended the scope of track detection methods. They demonstrated the generality of the track formation mechanism due to any heavily ionizing radiation by observing tracks in a variety of insulators, including crystals, glasses, and plastics. In each case, the chemicals used and conditions applied for etching could be optimized for the best revelation of tracks. In 1975, when the classical treatise[5] by these authors appeared in print, the field of Solid State Nuclear Track Detector (SSNTD) research was firmly established and its use had sprawled over dozens of fields in the natural sciences, ranging from archaeology to geology, astrophysics, and nuclear physics. Another book[6] on the subject appeared a decade later, while the most recent monograph relevant to technological applications was published in 1990.[7] The wide-ranging interests of research and usage of SSNTDs can be better gauged by referring to the proceedings[8] of biennial conferences held on the subject since the early 60s.

In this article we confine ourselves to the discussion of heavy-ion reaction studies conducted by using SSNTDs. The physics of heavy ions has witnessed enormous growth in the preceding years. New reaction modes like subthreshold fusion, deep inelastic scattering, and quasifission have been identified. The multifarious aspects of heavy-ion reactions have been dealt with comprehensively in the seven volumes of *Treatise on Heavy Ion Science*.[9]

The fields of heavy-ion physics and SSNTDs crossed paths rather early in their formative years. The earliest report appeared in 1963, in which Price *et al.*[10] presented results on the observation of three heavy fragments regarded as evidence of so-called ternary fission, following the reactions Ar+Bi, U. They used mica and phosphate glass as their detector materials. A few years later, Fleischer *et al.*[11] suggested more strongly that the observation of three correlated tracks in $ThSiO_4$ crystal is due to ternary fission following the reaction (10 MeV/u) $^{40}Ar+^{232}Th$. Similar work was reported by Perelygin *et al.*[12] for the reactions (230–380 MeV) Ar+Au, Bi, Th. The study of track systematics of binary and ternary events was continued by different groups[13–22] in the following years. During the course of that work, events of higher multiplicity were observed. In fact, the proof that heavy-ion reactions lead to four,[14] five,[21] and six[22] heavy reaction products in the exit channel was first provided by using the SSNTD technique. In most of those studies, mica and special glasses (ZnP metaphosphate) were used as detec-

 1063-7796/96/020154-25$10.00

tors. Those early investigations had limited aims. The main emphasis was to prove experimentally the existence of a nuclear reaction mechanism which leads to more than two heavy fragments in the exit channel. An important result from those studies was that the probability of high multiplicity in the exit channel increases with increasing masses of the reaction partners. (The presence of light particles such as n,p,d,α, etc., is not considered in this context.) The interpretation of the basic reaction mechanism was, at best, purely qualitative. In the absence of quantitative spectroscopic results, the conclusions drawn were sometimes erroneous; e.g., the observation of three heavy fragments was interpreted by Fleischer *et al.*[11] as ternary fission of a compound nucleus; however, more detailed investigations of heavy-ion reactions later showed that fusion of very heavy nuclei at energies around 10 MeV/u resulting in the formation of a compound nucleus (with its complete momentum transfer) is unlikely. For nuclei with $A>40$ and incident energy 1–3 MeV/u above the Coulomb barrier, the dominant reaction channel is of dissipative nature.[23] This reaction process, called deep inelastic scattering, is characterized by conversion of a significant amount of injection energy to internal excitation energy with relatively insignificant mass exchange. Thus, the projectile and target, by and large, retain their identity. The excited projectile-like or target-like nucleus, or both of them, may undergo normal fission as a second reaction step, giving rise to three or four heavy fragments. This possibility of a sequential process was first discussed by Karamyan *et al.*,[24] using counter detectors in the study of ^{22}Ne and ^{40}Ar induced reactions on Au, Bi, Th, and U. Apart from the interpretation of Refs. 11 and 24, alternative reaction mechanisms were also suggested by other groups, e.g., multifragment breakup with consecutive fusion of two fragments,[25] fast breakup in the nuclear or Coulomb field,[26] etc. Most of these concepts were applied in a qualitative sense to the multiparticle events observed with SSNTDs.[27]

The early attempts to derive quantitative information with a track detection system were based on theoretical velocity–range relations; e.g. Ait-Salem *et al.*[28] used the track data of fission fragments in the reaction ^{nat}U(n_{th},f) to derive masses and energies. Remy *et al.*[29] determined the masses and energies of reaction products produced by high-energy protons incident on different heavy target elements. Debeauvais and Tripier[30] studied, in the same manner, two-prong events, using deuterons as projectiles. The work of the Strassbourg group[31] is based on the parametrization of the theoretical velocity–range relation for certain detector materials, using α-particle ranges as a reference. In this external calibration it is assumed that the behavior of highly disturbed reaction products and detector material used for reaction studies would be identical to that of the projectile and detector material employed for calibration.

A completely different and more satisfactory method of calibration, developed at Marburg,[21] can be designated as internal calibration. In this method, the entire set of exclusive data measured in a kinematically complete manner is used for the purpose of calibrating an empirical velocity–range relation for heavy fragments in the exit channel of heavy-ion induced nuclear reactions. In this way the three-dimensional geometrical measurements of correlated tracks allow the determination of velocity vectors for all the fragments ensuing from the point of interaction. A complete kinematical analysis of multiprong events therefore becomes feasible in a simple and inexpensive manner with SSNTDs. The essential formalism of this method is discussed in Secs. 4.2.2. and 4.2.3. of the present article. It was first introduced and applied to the following heavy-ion reactions:[21]

(1535 MeV) ^{208}Pb+^{nat}U [Mica detectors],

(1785 MeV) ^{238}U+^{nat}U [Mica detectors].

This provided the first direct proof of the occurrence of sequential fission leading to three, four, and five particles in the exit channel of a heavy-ion reaction. A detailed description of the analysis and results for the reaction (806 MeV) ^{84}Kr+^{nat}U [Mica detectors] have been published.[32] In that report the details of the method were given, and the kinematical analysis was fully expounded. Through a detailed analysis it was found to be possible to establish the sequential fission process as the major reaction mode. The masses, energies, and centre-of-mass angles in both the first and the second reaction step were also determined. The use of this method was significantly broadened by later applications to the reactions[33–35]

(2149 MeV) ^{238}U+^{nat}U [Glass detectors],

(2149 MeV) ^{238}U+^{nat}U [Mica detectors],

(1050 MeV) ^{84}Kr+^{nat}U [Mica detectors].

In the last of the above reactions, some nonequilibrium effects, not observed at the lower energy of 806 MeV, were noted.

Obviously, the same multifragment reaction can be studied in an exclusive experiment and analyzed in a kinematically complete manner by using modern electronic detectors, fast coincidences, and associated computers. In recent years, there has been impressive progress in the development[36–39] and use[40–43] of electronic detectors with nearly 4π angular coverage. However, the SSNTDs offer a marked advantage in being simple and inexpensive, yet well suited for registering high-multiplicity events. The data are inherently exclusive and can be analyzed off-line, since the tracks are usually permanent under ordinary laboratory conditions. The portability of track detectors and minimal requirement of instrumentation (i.e., inexpensive chemicals, ordinary optical microscopes, etc.) mean that their use may be open to many laboratories of the world. There are some disadvantages of this method as well. The principal limitation is the number of analyzed events, which is usually rather limited, owing to the manual nature of the measurements. This obviously affects the statistical significance of the results. The wider use of automatic image-analysis systems is expected to overcome this shortcoming. In addition, at present the uncertainties in the measurement of individual tracks cannot be neglected and must be taken into account in the error analysis.

The experimental technique of registering the heavy-ion reaction products and revealing their tracks has been applied

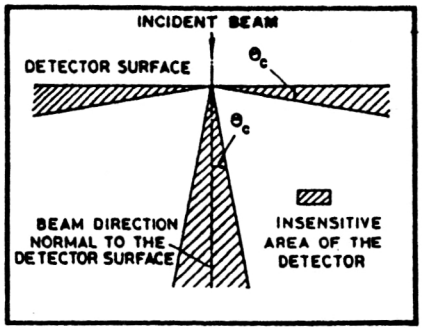

FIG. 1. "Sensitive" and "insensitive" angular intervals within an SSNTD. Tracks within the "critical" angular interval are not registered at all, or can be measured only with relatively large uncertainties.[46]

to a large variety of projectile–target combinations interacting at different energies (Refs. 21, 32–35, and 44–64).

The present review summarizes most of this work and also gives some unpublished data.

2. TRACK FORMATION AND REGISTRATION PROPERTIES

The formation of tracks in solid-state track detectors is very similar for protons, alpha particles, and heavy ions, and can be understood in terms of the "ion-explosion-spike" model.[65] The impinging positively charged ion loses its kinetic energy predominantly by the interaction with free and bound electrons within the absorbing medium. The dominant process is the ionization of K- or L-shell electrons. When the energy of the impinging ion is very low, nuclear stopping becomes important.[66] The details of the track formation depend on a variety of parameters, such as the mass, ionization state, and velocity of the incident ion, and the ionization potential of the absorbing material. Along the particle path a cylindrical zone is generated (50 to 100 Å in diameter), filled with positive ions. The positive ions repel each other, and consequently the density of the absorbing material is reduced in this region. This density reduction along the latent track has been directly observed by low-energy neutron scattering. The latent track has an increased chemical reactivity. A suitable etching medium can dissolve this region. The etching velocity along the track is higher than for the unirradiated material. This leads to an irreversible enlargement. The resultant track can be observed directly with an optical microscope.

It is important that a particle enters the detector at a certain angle with respect to its surface and that the actual track length exceeds a few μm; otherwise it would not be revealed after etching. Such a limitation in the registration of tracks is shown schematically in Fig. 1. The typical critical angle Θ_c with respect to the detector surface, for which the tracks are not observable, is in the range $\Theta_c < (3-10)°$. Furthermore, only particles heavier than a critical mass m_0 are registered in an SSNTD. The SSNTD technique therefore discriminates against light particles even at very high intensities. Details of the registration thresholds can be found in Ref. 5. Typical values for m_0 are as follows: for mica $m_0 = 30$ u,[14] and for metaphosphate glass $m_0 = 16$ u.[56] It is important for the kinematical analysis of nuclear reactions that the formation of latent tracks and their etching is isotropic. Exceptions are the critical angles mentioned above. The isotropic track-registration properties of glass and mica were shown experimentally in Refs. 56 and 57, respectively.

3. EXPERIMENT

3.1. The technique

In the investigation of heavy-ion reactions with mica and glass track detectors, the registration of events can be performed in the so-called 2π- and 4π-geometry techniques.[14] In the 4π-geometry technique the sandwich method is available. In this technique the target is sandwiched between two sheets of the detector material. The sandwich technique is particularly useful at higher bombarding energies, e.g., $E > 750$ MeV/u. A simple and very useful method in the study of heavy-ion reactions up to bombarding energies of $E_{lab} < 50$ MeV/u is the 2π technique:[27] The target material is vacuum-deposited (1–1.5 mg/cm^2) onto annealed mica foils or highly polished glasses.[12] Such targets are irradiated perpendicular to their surfaces with typical fluxes of about 10^6 heavy ions/cm^2. The flux and target thickness are optimized with respect to the number of registered events, the energy loss of the projectile in the target, spurious overlap of tracks, and the statistics of reaction products. In our work, exposures have been carried out at the following heavy-ion accelerators:

1. LINAC in Manchester (England);
2. ALICE in Orsay (France);
3. UNILAC in GSI, Darmstadt (Germany).

After the irradiation the target material is dissolved in HNO_3 or aqua regia. Afterwards, the solid-state nuclear track detector is properly etched so as to reveal the fragment tracks.[12,14,33] Then the sample is ready for study with the help of an optical microscope. The sensitive angular range is typically $5° < \Theta_{lab} < 85°$. For light projectiles of high energy and for heavy targets, this restricted 2π geometry in the lab system is nearly equal to a 2π geometry in the center-of-mass (c.m.) system. With increasing mass and energy of the impinging heavy ions, the experimental 2π geometry in the lab system approaches effectively a 4π geometry in the c.m. system. Particularly interesting in this regard are experiments using so-called inverted kinematics, i.e., heavy projectiles on light targets.[55] The experimental setup and some observed track correlations are shown in Fig. 2.

Typical patterns of multiprong events are shown as microscopic pictures in Fig. 3. Microphotographs of nuclear reactions leading to four-prong events (glass detectors) and five-prong events (mica detectors) are shown in Fig. 4. Tracks of impinging heavy ions which pass through the target without interaction are observable as dark spots in these figures. Multiprong events generated by nuclear reactions in the target layer and observed in the solid-state track detectors underneath can easily be recognized as such, as the common origin of all correlated tracks is in the target outside the SSNTD itself. Because of the restricted 2π geometry and the registration threshold of the detector, we sometimes miss the detection of fragments. Therefore, the true multiplicity of a

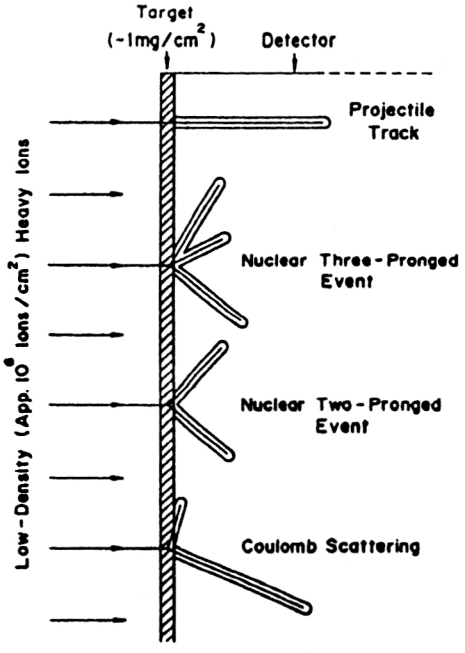

FIG. 2. Schematic representation of the 2π geometry used in SSNTD heavy-ion studies, together with the representation of some typical track configurations.[14]

multiprong event can be higher than the observed number of correlated tracks in a particular reaction. Typical examples of such so-called "indirect events" are shown in Figs. 3c and 3e.

For the quoted target layer thickness and heavy-ion flux, the density of two-prong events is typically of the order of 10^{-1} events/mm^2. The stochastic overlap of genuine two-prong events into an apparent four-prong event is smaller

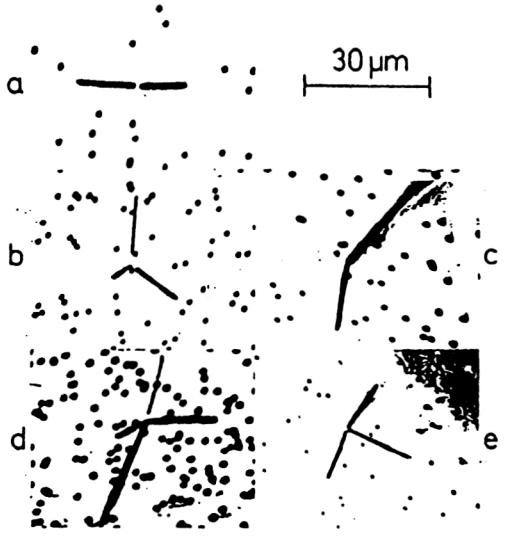

FIG. 3. Microphotographs showing tracks of projectiles (black dots) and (a) two-, (b) three-, and (d) four-prong events, respectively, as seen in the plane perpendicular to the beam (forward hemisphere). Also shown are typical examples of "indirect" (c) three- and (e) four-prong events. Here, at least one fragment for each multiprong event is scattered into the backward hemisphere, and is thus missing in the forward 2π geometry.[32]

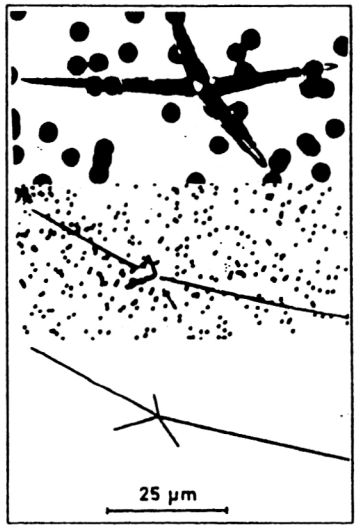

FIG. 4. The same as in Fig. 3 but for four-prong and five-prong events.[21]

than 10^{-4}. We can therefore disregard the artificial overlap of multiprong events.

The three-dimensional coordinates of correlated tracks due to multifragment interactions are measured using an optical microscope.[27] The flux of primary heavy ions is directly determined by counting the dots as seen in Figs. 3 and 4. The weight of the target material is determined with a microbalance by weighing the sample before and after depositing the target layer. In this way, our technique allows the direct determination of absolute interaction cross sections.

The number of multiprong events and their three-dimensional coordinates are the experimental raw data. Their analysis will allow us to determine the masses, energies, and momenta of the reaction products and the angles between individual fragment tracks and their mutual kinematical correlations. On the basis of these data one can obtain information concerning the reaction mechanism.

As a typical example of track-length and scattering-angle distributions, in Fig. 5 the respective distributions in the case of collinear two-prong events from the interaction (806 MeV) ^{84}Kr+^{nat}U are shown. (Collinearity within a plane normal to the beam is due to momentum conservation.) In Fig. 5 we can clearly differentiate the pair of tracks due to elastic scattering: short tracks (Fig. 5b) with $\theta_{lab}\sim 75°$ due to target-like uranium ions, and long tracks with $\theta_{lab}\sim 20°$ (Fig. 5a) due to projectile-like krypton ions.

3.2. Uncertainties

The uncertainties within the experimental raw data are due to several sources, e.g.:

1. Inaccuracies in the measurements of individual tracks.
2. Uncertainties due to straggling effects in ranges and angles.
3. Uncertainties due to the limited experimental geometry (2π).
4. Registration thresholds (e.g., $A \gtrsim 30$ u for mica).

For experiments performed so far, the following quantitative uncertainties have been reported:

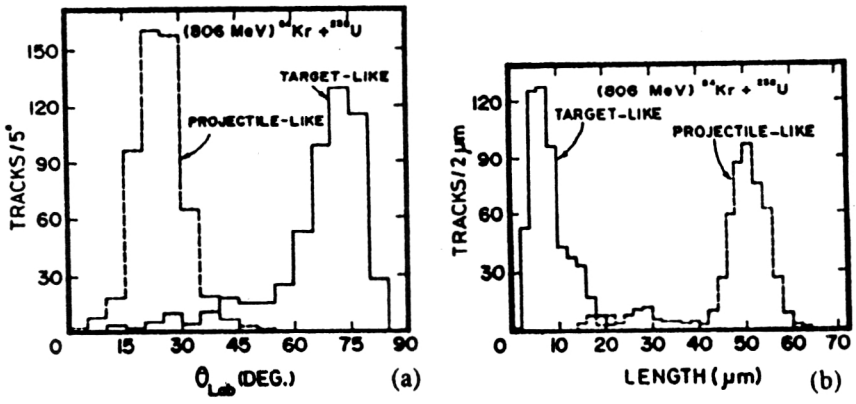

FIG. 5. Distribution of (a) scattering angles (lab) and (b) track lengths of correlated fragments in the two-body exit channel of ^{84}Kr+^{nat}U at E_{lab}=806 MeV. Note the experimental cutoff at forward angles.[32]

1. The total interaction cross section can be determined within uncertainties of about 13%. Only very rare events, say, five-prong events, are reported with a larger uncertainty due to their limited statistical occurrence.

2. The uncertainties in the projectile flux determination are usually about 8%. The uncertainties in the target thickness are determined to be about 6%. The statistical uncertainties in the determination of a certain category of multiprong events (multiplicity) are typically smaller than 5% when more than 400 events have been observed.

3. The uncertainty in the determination of the track lengths is ± 1.5 μm (standard deviation), and that of the angles is $\pm 2.5°$ (standard deviation). These uncertainties are typical for this type of work using an optical microscope. The track measurements in mica are somewhat more accurate than in glass. Certain classes of events, in particular those having ranges smaller than 5 μm, are associated with untypical large uncertainties. A detailed description of possible experimental uncertainties can be found in Refs. 27 and 68.

The uncertainties due to range or angular straggling effects are, in general, small compared with the uncertainties in the optical-microscope measurements.

Sometimes, in multiprong events we observe one very flat and short track. Calculations presented later show that these fragments were emitted backward in the c.m. system. Such tracks can barely be measured or calculated with any reasonable degree of accuracy.

Further systematic uncertainties will be described in due course in the following sections.

4. RESULTS AND CALCULATIONS

4.1. Investigated heavy-ion reactions and observed number of multiprong events

The heavy-ion reactions investigated so far are listed in Table I (Refs. 21, 32–35, 48, 55, 58, and 62–64). The different projectile–target combinations with incident energy (lab system) and the observed and analyzed 2-, 3-, 4-, and 5-prong events are presented in this table. The event numbers are divided into three classes. Class I refers to all the events of a particular reaction channel. We are here dealing with the total number of registered and counted events. These events will be used for evaluation of the total (absolute) cross section and for the differential angular distribution (elastic scattering). Class II refers to that subset which was measured completely (all spherical coordinates). Not all the events were suitable for a detailed quantitative analysis. Some of the events had to be rejected because of unusually large measurement errors (e.g., very shallow tracks, very steep tracks, failures in the target or in the detector, and tracks with end-points in the incident channel of a projectile particle). The events subject to quantitative analysis are designated as class-III events.

4.2. Kinematical analysis of multiprong events

4.2.1. Completeness

A reaction with N (spinless) particles in the final channel is completely determined by N individual momenta and N individual masses. These $4N$ variables reduce to $4(N-1)$ kinematically independent variables via momentum conservation and (cylindrical) symmetry around the beam axis (unpolarized beam).

The three-dimensional coordinates of coincident multitrack events provide 4, 8, 11, and 14 independent quantities for the 2-prong, 3-prong, 4-prong, and 5-prong events, respectively. These independent experimental raw data are the track lengths and the track angles between the tracks and the beam axis, and the track angles between the tracks in the plane perpendicular to the beam. These experimental data are kinematically complete for the 2-prong and the 3-prong events. For the 4-prong events one kinematic quantity is missing, and for the 5-prong events two kinematic quantities are missing. The kinematics of the 4-prong and 5-prong events can therefore be analyzed only with additional assumptions. A realistic assumption is the conservation of the total mass for the 4-prong events, and, in addition, the parametric input of one sum of the masses of two arbitrary fragments for the 5-prong events. By this procedure one missing kinematic variable for the 4-prong and two missing kinematic variables for the 5-prong events can be generated, and a complete kinematic analysis can be carried out.[21,32]

TABLE I. Investigated nuclear reactions, number of registered multiprong events, and number of events analyzed kinematically.

Reaction		2-prong events			(3)	3-prong events			(4)	4-prong events			(5)	5-prong events		
		I	II	III		I	II	III		I	II	III		I	II	III
$^{235}U(n_{th},f)$[2]	*A*	108	108	108	···	···	···	···	···	···	···	···	···	···	···	···
(540 MeV) $^{84}Kr+^{nat}U$[2]	*A*	67	67	67												
(806 MeV) $^{84}Kr+^{nat}U$	*A*	496	206	178	347	149	131	110	4	1	1	1	···	···	···	···
(1050 MeV) $^{84}Kr+^{nat}U$	*A*	650	650	600	648	167	120	80	7	3	3	2	···	···	···	···
(1539 MeV) $^{208}Pb+^{nat}Pb$	*A*	200	1)		···	47	1)		···	3	3	3	···	···	···	···
(1535 MeV) $^{208}Pb+^{nat}U$	*B*	294	294	283	5	72	70	51	11	13	10	10	···	···	···	···
(2380 MeV) $^{238}U+^{165}Ho$	*A*	500	500	1)		1)				1)				1)		
(2380 MeV) $^{238}U+^{197}Au$	*A*	500	500	1)		1)				1)				1)		
(2380 MeV) $^{238}U+^{209}Bi$	*A*	500	500	1)		1)				1)				1)		
(1785 MeV) $^{238}U+^{nat}U$	*A*	270	270	270	23	439	154	154	25	373	193	137	···	1	1	1
(2149 MeV) $^{238}U+^{nat}U$	*B*	540	540	180	···	150	116	93	···	212	205	136	···	1	1	1
(2149 MeV) $^{238}U+^{nat}U$	*A*	130	130	130	13	174	158	148	27	251	210	141	2	···	···	···
(2380 MeV) $^{238}U+^{nat}U$	*B*	1)				64	57	46	14	87	80	80	···	···	···	···
(3975 MeV) $^{238}U+^{nat}U$	*A*	800	200	1)	337	815	1)		375	332	1)		14	22	1)	

Legends:
(1): Not investigated
(2): Only for calibration
(3): Indirect 3-prong events
(4): Indirect 4-prong events
(5): Indirect 5-prong events
(−): Not observed
A: mica detector
B: glass detector
I: number of registered events
II: number of events whose geometrical properties were fully determined experimentally
III: number of events completely analyzed kinematically

The momentum conservation does not impose any constraints on the specific type of interaction between the particles participating in the nuclear reaction. The kinematic completeness implicitly assumes an unpolarized beam as given by the experimental setup and the neglect of spin–orbit interactions of the reaction products. The mass conservation implies that all the reaction products have been detected. Thus, in particular, owing to the finite detection threshold and the restricted solid angle, certain constraints arise in the methodology for the analysis of the 4- and 5-prong channels.

4.2.2. Conversion of track parameters into fragment masses and energies

Experimental investigations, semi-empirical methods, and theoretical considerations[4,67–72] show that a relation of the form

$$v_i = v_i(R_i, m_i, Z_i) \tag{1}$$

exists between the range R_i and the velocity v_i of the track producing particle i (for a given solid stopping medium). Here m_i and Z_i are the mass and charge of the ith particle, respectively. For practical purposes, the form frequently used is[73–75]

$$R_i = k_i . v_i^{\nu} \quad \text{with} \quad k_i = k_i(m_i, Z_i) \tag{2}$$

with ν as a free parameter. For not too high velocities, Lindhard *et al.*[66] have shown that $\nu = 1$ in the above equation if the electronic stopping is the dominant process.

The charge dependence of k_i according to Ref. 66 is given by

$$k_i = Z_i^{1/6} f(m_i, M)/[1+(Z_i/Z)^{2/3}]^{3/4}, \tag{3}$$

where Z and M are the mean charge and mass of the atoms of the stopping medium. There exist arguments in the literature[76–80] that the value of k_i for different particles fluctuates around the value given by Eq. (3). The reasons for these fluctuations can be attributed to the effects caused by the atomic shell structure.

For our purposes it is, however, important to note that the explicit dependence on the charge of the track producing particles for constant mass m_i and given stopping medium is extremely weak ($\sim Z_i^{1/6}$). A genuine test of the charge dependence of ranges of different isotopes is very difficult for practical reasons. Possible variations are often hidden by experimental uncertainties. This is all the more true in the present investigations of highly perturbed fragments issuing from heavy-ion reactions and the limited accuracy in the measurement of their ranges. Neglecting the explicit weak charge dependence in the subsequent analysis, we therefore use the relation

$$v_1 = v_i(R_i, m_i). \tag{4}$$

To every track t_i we can assign a range R_i (i.e., its length) and a direction $\bar{e}_i$. Using Eq. (4) and the requirement of momentum conservation, it follows that

$$\sum_{i=1}^{N} m_i v_i(R_i, m_i)\bar{e}_i = \bar{P}_{in}, \tag{5}$$

where P_{in} is the total momentum and N is the multiplicity of the event under consideration.

The kinematic method of track analysis is based on the solution of the system of equations (5), event by event, where the general analytical form $v(R,m)$ used in Refs. 21, 32, and 35 is

$$v(R,m) = \sum_{\mu=0}^{2} \sum_{\nu=0}^{4} c_{\mu\nu} m^{\mu} R^{\nu}. \tag{6}$$

The coefficients $c_{\mu\nu}$ are determined by an internal calibration procedure discussed later. With measured R_i and $\bar{e}_i$,

given total momentum $\bar{P}_{in}$, and given coefficients $c_{\mu\nu}$, the system of equations (5) is solvable for the unknown masses m_i. In a second step, these values are used in Eq. (6) for the measured values of R_i, and each velocity v_i is determined. Then from the measured directions, $\bar{e}_i$, the velocity vectors $\bar{v}_i$ of the particles are known, and therewith all relevant kinematic quantities like kinetic energies, momenta, relative momenta of particles in different reference systems, etc.

For 4-prong events, in addition to Eq. (5), a subsidiary condition is imposed, i.e.,

$$\sum_{i=1}^{4} m_i = m_P + m_T, \tag{7}$$

where m_P and m_T are the projectile and target masses, respectively.

For 5-prong events, a further condition is required. In the present work, the sum of the masses of two arbitrary fragments to be held fixed is used as a constraint for intermediate masses, i.e.,

$$m_i + m_j = m_{ij} = m \quad (m \text{ chosen as a free parameter}). \tag{8}$$

This relation is taken as a trial value of m_{ij}. With such an additional constraint the coupled equations (5) and (6) are solvable, and again all the relevant kinematical variables can be obtained. The resulting kinematical variables depend (parametrically) on the initial (trial) value m_{ij}. By varying this trial value within physically reasonable limits and changing the ten possibilities of grouping five fragments into pairs (ij) (klm), one and only one solution of Eqs. (5) and (6) was found for all the analyzed 5-prong events. This solution is characterized by the fact that all the computed masses are positive ($m_i > 0$ for all i, $i = 1, 2, 3, 4, 5$) and are larger than the registration threshold of the detector, e.g., 30 u for mica or 16 u for glass.

Since light particles are not registered in the solid-state track detectors, no experimental information is available on them. Consequently, these cannot be explicitly incorporated in the analysis. On the other hand, it is obvious that the initially well defined kinematic relations between the primary fragments might be perturbed for the secondary fragments after the emission of light particles (for details, see Ref. 32).

Two questions arise in this connection. First, Eq. (5) is based on absolute momentum conservation, whereas the secondary fragments fulfill this condition only approximately. Second, the track data are related to the secondary fragments; however, the masses of the primary fragments are of interest to us. In Ref. 32 it was shown that the kinematic determination of fragment masses and fragment momenta from the velocities of the *secondary* fragments and the total incident momentum provides, to a good approximation, the masses of the *primary* reaction products before the emission of the light particles. The relative error in the computed masses, in a first approximation, is given by

$$\delta m / \Delta m_i = -(\varepsilon/\varepsilon + 1)(1 + 0.5\eta + (\Delta m / m_i)),$$

$$\text{with } \varepsilon = m_i v_i' / v_i, \quad \eta = m_i v_i'' / v_i'. \tag{9}$$

Here δm denotes the difference between the computed mass m_i and the true (primary) mass, and Δm is the difference between the primary and the secondary mass; v_i' and v_i'' are the first and second partial derivatives of the velocity $v(R,m)$, [Eq. (6)] with respect to the mass. The difference δm vanishes for mass-independent velocity–range relations. Velocity–range relations are, in general, only weakly dependent on the mass. For the actual velocity–range relation [Eq. (6)], it turns out[32] that $\varepsilon \cong 10^{-1}$, $\eta \cong 1$. The value of δm is therefore an order of magnitude smaller than Δm.

Further, the conclusion that δm is a positive quantity (i.e., $\varepsilon < 0$) is of interest. The algorithm described above therefore somewhat overestimates the primary masses.

The reasons for the validity of the above procedure for kinematic track analysis for all practical purposes are twofold. First, the light particles (e.g., n,p, etc.) are emitted isotropically in the fragment c.m. system (evaporation). This has been verified for heavy-ion reactions, from deep inelastic to quasi-inelastic reactions.[81] Second, although the primary and secondary fragments have different masses, they have the same mean velocities. Because of the weak dependence of the velocity–range relation on the mass, the differences in the ranges are small for fragments with equal velocities. A necessary prerequisite is, however, that the spectrometry is based on velocity measurements and not on energy measurements.[82]

Although the isotropic evaporation of light particles does not decisively influence the kinematic spectrometry, it nevertheless leads to a further broadening of the resulting mass, momentum, and energy distributions. The mean values remain unchanged, but the dispersions increase. The inherent dispersion is small for fragments with high velocities, as is the case with most of the investigated heavy-ion reactions.

4.2.3. Velocity–range relation and its calibration

Velocity–range relations can be determined by independent measurements. They are also obtainable through internal calibration. Both of these methods have been applied in Refs. 21, 32–35, and 58. Internal calibration turned out to be the preferred method.

Independent calibration. From independent investigations the velocity–range data are known for different heavy-ion systems at different energies.[56,68,83–86] In addition, extrapolations are available on the basis of semi-empirical and theoretical models.[31,69,87–89]

Figures 6 and 7 show the experimental values of the ranges at different energies for glass and mica detectors, respectively. Figure 7 also shows the predictions of Northcliffe and Schilling[69] for a chosen ion mass. Bragg's additivity theorem was applied in the calculations of the semi-empirical curve for mica as the stopping medium.[69,90] Bragg's theorem relates the stopping power of a compound to its individual constituents. The elements given in Ref. 69 have been incorporated in accordance with the detector composition. Also considered is the fact that heavy ions with velocities below a critical threshold do not produce etchable disturbances in glass or mica. The semi-empirical ranges cal-

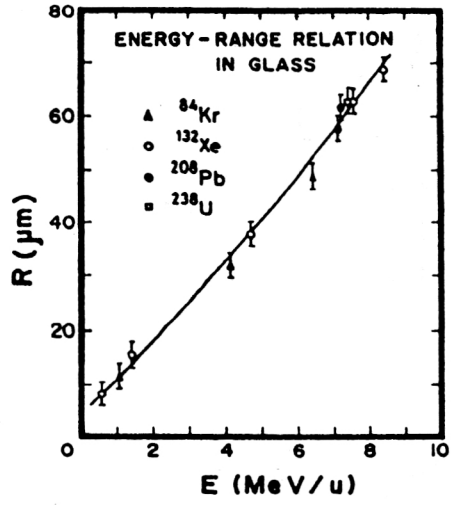

FIG. 6. Empirically determined ranges in ZnP glass detectors for a variety of heavy ions. The ranges are shown as a function of the energy per nucleon. The line shown is a mass-independent χ^2 fit to the experimental data.[56]

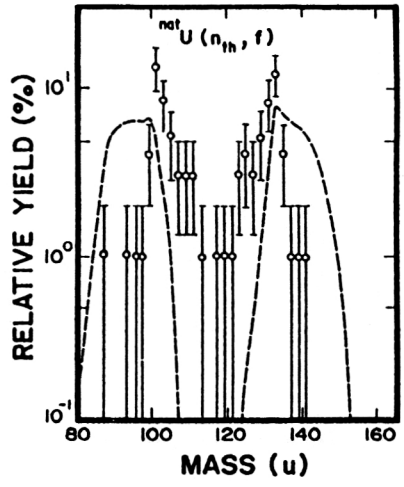

FIG. 8. Mass-yield curve for fission fragments from thermal-neutron induced fission of ^{235}U. The SSNTD data were converted with the help of a mass-independent velocity–range relation. The uncertainties quoted are due to statistical uncertainties.

culated from the table are thus corrected for their etchable component. Because of the small number of measured points and the experimental uncertainty, it is not possible to evaluate reliably the eventual mass dependence by such independent calibration. Further, it can be seen that the semi-empirical ranges reproduce the experimental data only in a limited manner. The semi-empirical Northcliffe–Schilling data have to be corrected by about 13% to 20%. This is well known for other stopping media.[91] In this situation it seems reasonable to restrict oneself to mass-independent velocity–range relations, which might be extracted by a χ^2 fit to the measured ranges.

The mass distribution of fission fragments from ^{235}U(n_{th},f) is shown in Fig. 8. It was obtained with the help of kinematic conversion of track parameters and a mass-independent velocity–range relation. Also shown in Fig. 8 are the experimental fragment mass distributions (dashed curve) which have been extracted by radiochemical methods.[92]

The SSNTD experimental mass distribution is narrower than the radiochemical data. Also, the mass-maximum of the lighter fragments of the track data is displaced towards the mass-maximum of the heavier fragments, when compared to the radiochemical data. Both trends are unreasonable. In fact, the track data contain experimental errors as well as further uncertainties from angular, energy, and range straggling. Neutron evaporation also leads to a further dispersion in the track data. The track data thus should have yielded significantly broader distributions than the ones from the radiochemical data. Since the χ^2 distribution measured radiochemically may be regarded as the exact one, it therefore follows that the mass independence of the energy–range relation is an inadmissible simplification. Similar effects, namely, too narrow distributions and systematic displacements of light fragments towards the heavier mass peak, are also known from other spectrometric fission-fragment investigations with solid-state track detectors and mass-independent velocity–range relations.[93] Too narrow distributions and systematic shifts of heavy and light particle channels have been likewise observed in the heavy-ion reaction (1535 MeV) ^{208}Pb+^{nat}U for the 3-particle and 4-particle channels[56] if the analysis is performed by means of a mass-independent energy–range relation.

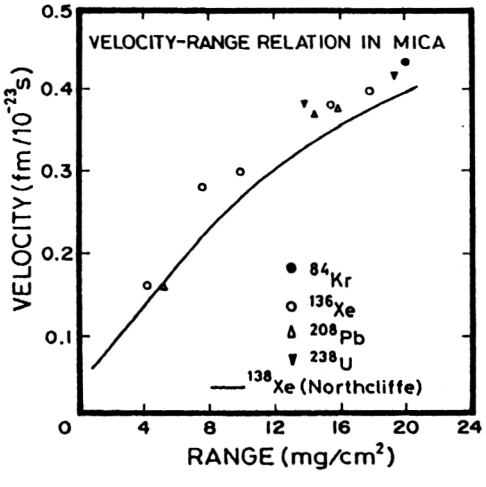

FIG. 7. Empirically determined ranges in mica (muscovite) detectors for a variety of heavy ions as a function of their velocity in the lab system. The line drawn is based on Northcliffe and Schilling's tabulations[69] for ^{138}Xe. The experimental data are taken from Ref. 68.

Mass-dependent internal calibration. Figures 9 and 10 show the mass distribution and the total kinetic-energy distribution when a mass-dependent optimized velocity–range relation is employed for the situation discussed with respect to Fig. 8. The broken curve in Fig. 9 corresponds to the above-mentioned radiochemical data. The solid curve arises from the folding of the radiochemical data with a mass uncertainty of $\sigma_m = 7$ u. The broken curve in Fig. 10 refers to counter experiments.[94] The solid curve is a least-squares fit to the track-detector data under the assumption of a linear dependence of the fragment energies on the mass ratio be-

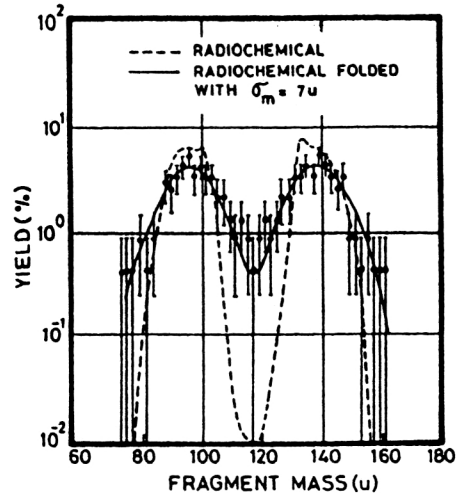

FIG. 9. Fission-fragment mass-yield curve for thermal-neutron induced fission of ^{nat}U, obtained by conversion of the track data based on a mass-dependent velocity–range relation. The dashed line corresponds to radiochemical data. The solid line refers to radiochemical data which are modified by the experimental uncertainty of this work ($\sigma_m = 7$ u).[32]

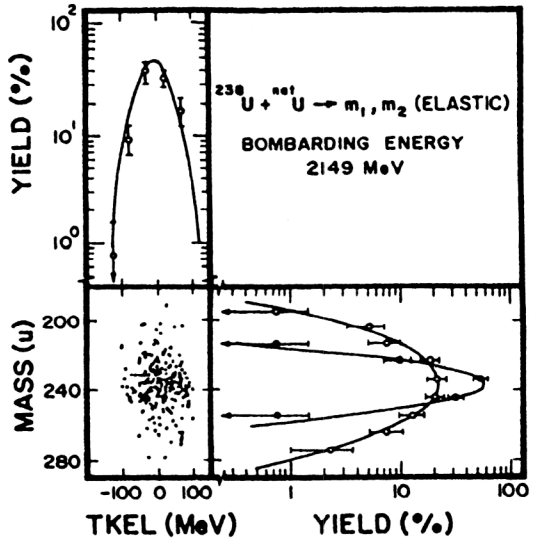

FIG. 11. Correlation plot of individual fragment masses with respect to their energies for elastic scattering in the reaction (2149 MeV) $^{238}U+^{nat}U$. The conversion of track lengths is based on an optimized, mass-dependent velocity–range relation. Only statistical uncertainties are given.[58]

tween the lighter and the heavier fission products.

The coefficients of the mass-dependent velocity–range relation are obtained by a suitable choice of the coefficients in Eq. (6), based on an optimal fit to the light and heavy mass peaks as well as the mean kinetic energy of the fission fragments. Figures 9 and 10 demonstrate that by this kind of internal calibration, fission-fragment tracks can be analyzed consistently and converted into fragment masses and fragment energies.

An analysis of the two-particle channel in heavy-ion reactions, by fitting of the coefficients found from $U(n_{th},f)$ to the projectile and target mass as well as to the elastic line in heavy-ion scattering, yields, in general, optimal velocity–range relations for all interesting masses, energies, and ranges. Figures 11 and 12 demonstrate the adequacy and internal consistency of these procedures.

For the 2-particle and 3-particle channels, the mass conservation

$$\sum_{i=1}^{N} m_i = m_P + m_T \quad (N=2,3) \tag{10}$$

(m_P=projectile mass; m_T=target mass) is not used in the calibration. Consequently, a further check is provided by the comparison between the calculated sum of the fragment masses and the total mass of the projectile and target. This is demonstrated for the reaction (1785 MeV) $^{238}U+^{nat}U$ (2- and

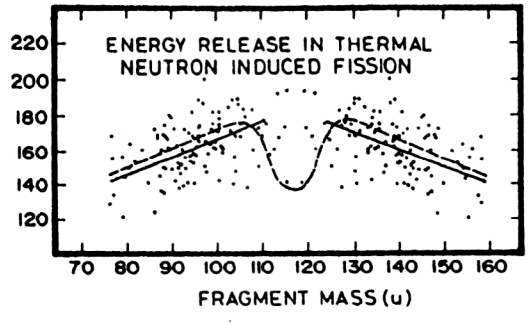

FIG. 10. Distribution of total fission-fragment energies versus mass split. The conversion of track data is based on the mass-dependent velocity–range curve. The dashed line refers to counter experiments,[94] and the solid line is the regression line for the data, assuming a linear dependence on the mass split.[32]

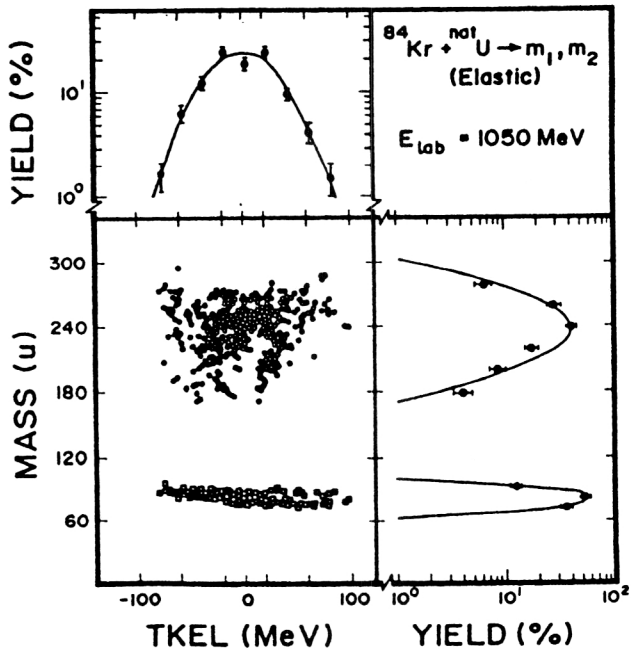

FIG. 12. Correlation plot for the masses of the two-body exit channel and the TKEL. The data correspond to elastic (+ quasi-elastic) binary events and are uncorrected for experimental uncertainties. The masses and energies were calculated using an optimized mass-dependent velocity–range curve (see Fig. 15).[96]

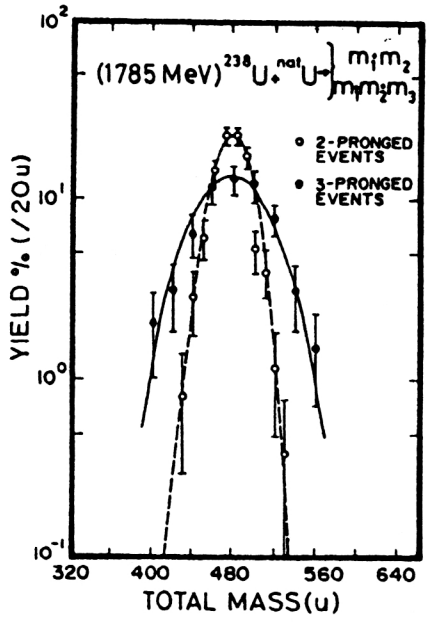

FIG. 13. Distribution of the sum of the fragment masses in the 2-particle and 3-particle exit channels for the reaction (1785 MeV) $^{238}U+^{nat}U$. The distributions are Gaussian with mean value 476 u and standard deviations $\sigma_{2m}=17.2$ u (2-particle exit channel) and $\sigma_{3m}=35.4$ u (3-particle exit channel).

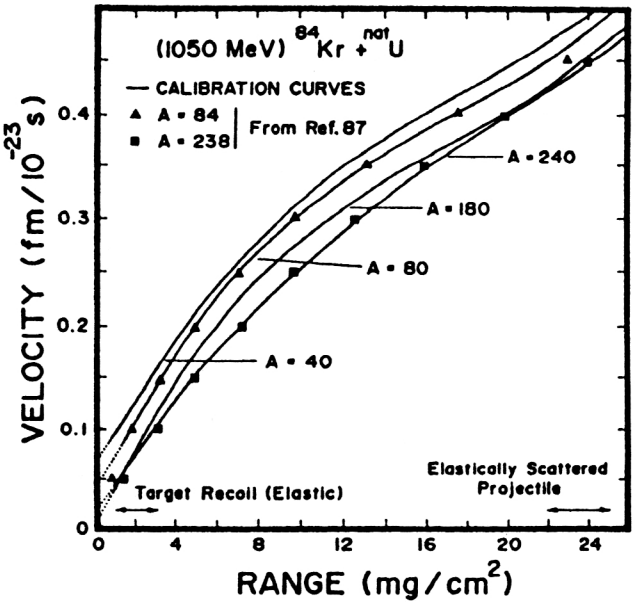

FIG. 15. Empirical velocity–range curves obtained after performing internal calibration. For comparison, the calculations based on Ref. 87 are also shown. The regions of the curves which are most sensitive for fitting the projectile and target masses are indicated by horizontal bars with arrows.[35]

3-particle channels) in Fig. 13. The agreement between the calculated and expected values is satisfactory. The authors of Refs. 21, 33, 45, and 54 arrive at the same conclusions.

Typical velocity–range relations found from internal calibration are shown in Figs. 14 and 15 for mica detectors. Also shown in Fig. 14 is the upper theoretical limit for the region of proportionality between the velocity and the range. One can see that this region is narrower than that predicted. This is particularly true for very heavy ions ($A>200$ u). The velocity–range relation obtained by Qureshi *et al.*[35] (Fig. 15) in the case of the (1050 MeV) Kr+U reaction observed with mica detectors was also compared with the calculations based on Benton and Henke's theoretical model.[87]

The velocity–range relations found in this way are calibration polynomials. They are valid only within their well-defined limits. They represent the best curves for the investigated track-length distributions, special detectors, etching conditions, and particular track-producing particles. These are therefore not suitable for extrapolations beyond their respective limits. Experience showed that for every new experiment and for each new track detector at hand, a new internal calibration had to be carried out.

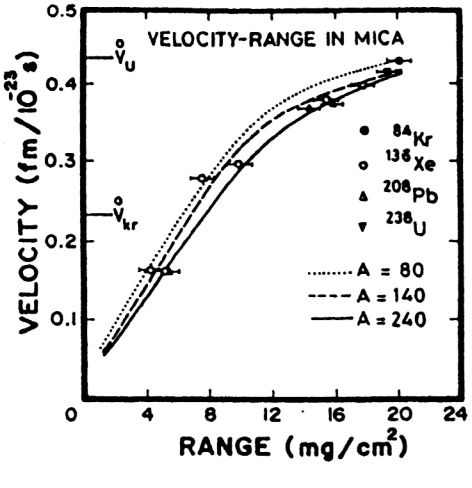

FIG. 14. Comparison of empirical velocity–range curves of this work for some selected nuclei with directly measured data. For the nuclei ^{84}Kr and ^{238}U we also indicate the upper limits ($\hat{v}_{Kr}$ and $\hat{v}_U$, respectively) for the theoretically predicted region of velocity-proportional stopping.[32]

4.2.4. Error analysis and data selection

The largest (relative) errors in the ascertained physical quantities arise from the lighter fragments and from fragments with very short tracks. This is a particular characteristic of the kinematic track analysis.

The uncertainties have been ascertained with different methods. The influence of the measurement uncertainties have been simulated by Monte Carlo methods as follows: Within the experimental uncertainties the track lengths and track angles are varied for randomly selected multiprong events. In this way, new data sets are generated event-by-event in the form of distributions. Their half-widths are a measure for the experimental error. Figure 16, e.g., shows such a statistically generated distribution for the 4-prong event in (806 MeV) $^{84}Kr+^{nat}U$.

In the kinematic analysis of multiprong events there are also further errors besides the measurement errors. Most important are the inaccuracies because of straggling, evaporation of light particles, errors in calibration, and differences in etching procedures and etching behavior.

An estimate of the influences of all these errors can be obtained from the width of the elastic peak (Q value, projec-

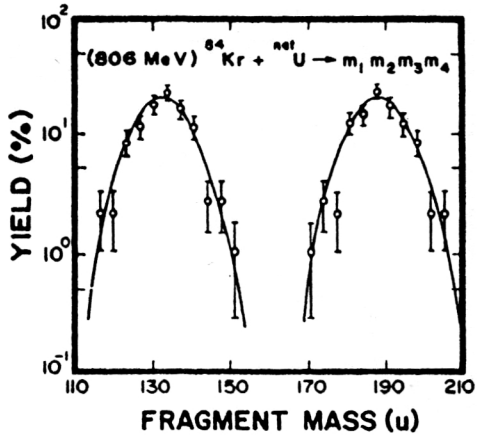

FIG. 16. Errors in the prefission masses of the observed four-prong event in (806 MeV) ^{84}Kr+^{nat}U as obtained by a Monte Carlo simulation of the inaccuracy in the track-length and track-angle measurements.[32]

tile mass, target mass) and from the width of the sum of the fragment masses in the 2-prong and 3-prong channels. Such distributions are shown in Figs. 11 and 12.

It turns out that the distribution of the total fragment mass in the 3-prong channel is significantly broader than that in the 2-prong channel. This behavior has been found in all the reactions. It can be traced back to the increasing number of independent quantities to be measured with increasing multiplicity of the reaction. If it is assumed that the errors of the individually measured quantities enter with equal weight into the final quantities, then to first order the uncertainties scale as the square root of the number of independent variables. On the average, a relative error of 3.3% (standard deviation) can be deduced per degree of freedom for the determination of the masses. It varies from 2.0% to 4.6%, depending on the reaction under investigation and on the applied detector.

The actual analysis in Refs. 21, 32–35, and 58 as well as in this work is restricted to events in which the sum of the fragment masses in the exit channel was within two standard deviations of the expectation value. For the 4-prong and 5-prong events a condition was imposed that the evaluated masses of the fragments are above the registration threshold of the detector. The subset III of Table I refers to this restricted set. In Ref. 34 the selection was based on an additional criterion. Only those events were analyzed in detail, for which the relevant kinematic variables allowed the conclusion of a sequential process.

4.3. Total and partial reaction cross sections

A list of measured total reaction cross sections and partial reaction cross sections for individual multiplicities is given in Table II. These have been calculated according to the equation

$$\sigma_i = R_i/\Phi A, \tag{11}$$

where R_i is the number of events of multiplicity i observed per unit surface area, A is the number of target nuclei per unit surface area, and Φ is the flux of incident ions.

The 2-particle exit channel has only been included for inelastic events with TKEL>100 MeV. The experimental total reaction cross section is the sum of the partial reaction cross sections for the 2-, 3-, 4-, and 5-particle channels. The quoted uncertainties include the statistical uncertainty as well as the errors in the measurement of the flux and the number of target nuclei. Typical relative errors in these measurements are about 10%. The so-called "indirect" events with n observed particles have been included in the $(n+1)$ class. $\sigma_R^{(1/4)}$ is the total reaction cross section, based on the experimentally observed quarter-point angle $\theta^{(1/4)}$ and calculated according to Frahn's Fresnel model.[97] The uncertainties in $\sigma_R^{(1/4)}$ are strictly those due to statistical uncertainties and uncertainties in the experimental determination of the quarter-point angle. The total error might be larger, owing to the difficulties in separating elastic and quasi-elastic events experimentally.

The 2π detector geometry used in this work has an obvious limitation: When we observe n fragments in one interaction, there could have been $(n+x)$ fragments in reality, with x fragments emitted in the backward direction. Therefore, we consider only those events with n observed fragments as being due to the n-particle exit channels when these

TABLE II. Total and partial reaction cross sections.

Reaction	σ_R	$\sigma_R^{(1/4)}$	σ_2	σ_3	σ_4	σ_5	Ref.
(806 MeV) ^{84}Kr+^{nat}U	2410±390	2680±290	150±35	2235±340	23±11		32
(1050 MeV) ^{84}Kr+^{nat}U	3201±282	3389±110	···	3185±278	16±6	···	35
(1539 MeV) ^{208}Pb+^{nat}Pb	(2)	(2)	(2)	(2)	(2)	···	49
(1535 MeV) ^{208}Pb+^{nat}U	(2)	1650±250	(2)	1100±130	200±70	···	21
(2380 MeV) ^{238}U+^{165}Ho	(2)	2970	(2)	(2)	(2)	···	55
(2380 MeV) ^{238}U+^{197}Au	(2)	2900	(2)	(2)	(2)	···	55
(2380 MeV) ^{238}U+^{209}Bi	(2)	2780	(2)	(2)	(2)	···	55
(1785 MeV) ^{238}U+^{nat}U	1840±250	1640±120	···	980±130	850±110	10±7	48
(2149 MeV) ^{238}U+^{nat}U	2930±380	2970	···	1110±140	1810±240	9±6	33
(2149 MeV) ^{238}U+^{nat}U	3050±390	2800±240	···	1210±170	1830±240	14±10	58
(2380 MeV) ^{238}U+^{nat}U	2670	(2)	(2)	900)	1720	35	45
(3975 MeV) ^{238}U+^{nat}U	4740±570	4880±700	···	2880±350	1770±220	90±20	58

σ_R: Total experimental reaction cross section (sum of σ_2, σ_3, σ_4, and σ_5)
$\sigma_R^{(1/4)}$: Total experimental reaction cross section determined with the help of elastic scattering and quarter-point angle
(2): not investigated in detail
-: not investigated at all

TABLE III. Comparison of experimental and theoretical reaction cross sections.

Reaction	$\sigma_R^{(1/4)}$ (mb)	σ_R^{Blair} (mb)	$\sigma_R^{\text{opt.}}$ (mb)
^{238}U+^{165}Ho (2380 MeV)	2970	3360	3220
^{238}U+^{197}Au (2380 MeV)	2900	3320	3200
^{238}U+^{209}Bi (2380 MeV)	2780	3320	3210

$\sigma_R^{(1/4)}$: Total experimental reaction cross section determined through the elastic-scattering quarter-point angle

σ_R^{Blair}: Reaction cross section calculated with the help of the sharp-cut-off model (Blair)

$\sigma_R^{\text{opt.}}$: Reaction cross section calculated with the help of the optical model

events are amenable to kinematic analysis for the relevant multiplicity. Other cases are considered as "not having been analyzed kinematically." Therefore, the values given in Table II are lower limits for high multiplicities (i.e., $n=4$ and $n=5$) and upper limits for low multiplicities (i.e., $n=2$ and $n=3$).

As shown in Table II, the sum of the partial cross sections for the 3-, 4-, and 5-particle exit channels agrees fairly well with the total interaction cross section determined independently via the quarter-point angle $\theta^{(1/4)}$. This is a reassuring experimental result.

Experimentally determined total interaction cross sections can also be compared with theoretical calculations based on the optical model or on the "sharp-cutoff" model of Blair.[98] This gives an independent check on the reliability of the results obtained so far. The most detailed calculations have been carried out, in this respect, for the systems (2380 MeV) ^{238}U+^{165}Ho, ^{197}Au, and ^{209}Bi (Ref. 55). In the optical-model calculations, a conventional Woods–Saxon parametrization according to Thomas[99] with $r_0=1.28$ fm as the radius parameter for the nuclear potential V_N was used. The interaction parameter R_{int} and the interaction barrier B_{int} in the "sharp-cutoff" model were calculated using additionally the proximity and droplet model as follows[100,101] (P =projectile; T=target):

$$R_{\text{int}}/\text{fm}=0.8425(C_P+C_T)+4.49, \tag{12}$$

$$C_i=r_i(1-1/r_i^2),$$

$$r_i/\text{fm}=1.28A_i^{1/3}-0.76+0.8/A_i^{1/3},$$

$$B_{\text{int}}/\text{MeV}=(Z_PZ_Te^2/R_{\text{int}}-0.1024\gamma\exp(2.7-\xi)/0.7176), \tag{13}$$

$$\gamma=11.959[C_PC_T/(C_P+C_T)][1-1.7826\{1-2(Z_P+Z_T)/(A_P+A_T)\}^2],$$

$$\xi=4.49-0.1575(C_P+C_T).$$

The experimental and theoretical results are shown in Table III. The results obtained by different models agree reasonably well with each other. The experimental and theoretical values also agree fairly well, considering the experimental uncertainties. It may, however, be noted that in Table III the experimental cross sections are systematically somewhat smaller than those calculated. We do not put too much emphasis on this difference, since it might be due to inherent limitations of the experimental 2π-geometry technique, as pointed out earlier. In particular, if elastic as well as quasi-elastic binary events are counted as being due to elastic scattering, then one overestimates $\theta^{(1/4)}$ and thus calculates too low a value for the cross section $\sigma^{(1/4)}$. Consequently, one obtains also too low a value for σ_R, which involves the sum of all observed multiprong events ($n=2,3,4,5$).

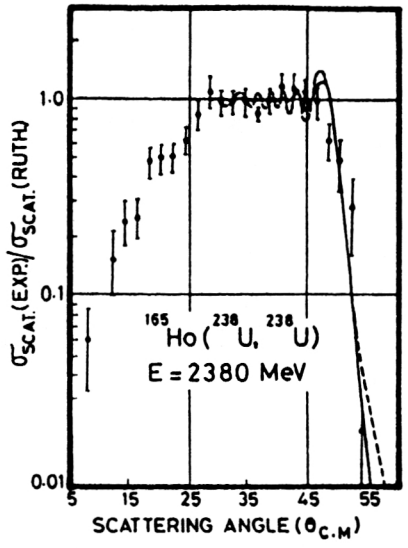

FIG. 17. Angular distribution in the elastic scattering for the reaction (2380 MeV) ^{238}U+^{165}Ho. The ratio of differential cross sections between the observed and Rutherford scattering is given. The deviation for $\theta_{\text{c.m.}}<25°$ is due to inherent technical biases of the 2π-geometry technique. The lines are drawn according to the Fresnel model (see the text). Only statistical uncertainties are given.[55]

4.4. Elastic scattering and reaction parameters

A typical angular distribution for two-prong events due to elastic scattering is shown in Fig. 17. The ratio of the experimental differential cross section divided by the calculated Rutherford cross section as a function of the scattering angle is shown for the reaction (2380 MeV) ^{238}U+^{165}Ho. Similar results have been obtained for other systems.[55] The quoted experimental uncertainties are strictly statistical. As mentioned earlier, the inclusion of quasi-elastic events could have introduced a systematic error. We defined all binary events as being due to elastic scattering, when $\Delta m/m=7\%$ and $\Delta E/E=4.5\%$ within the elastic reaction kinematics. Figure 17 is based on absolute values for the differential cross sections, since the total target thickness and the total heavy-ion flux are directly measured. Technical reasons are responsible for the underestimation of elastic scattering for $\theta_{\text{c.m.}}<25°$. For uranium-induced reactions, in the angular range $25\leqslant\theta_{\text{c.m.}}\leqslant50°$ one observes rather pure Rutherford scattering; here we are in the domain of rather large impact parameters between the target and projectile. For the scattering angle $\theta_{\text{c.m.}}>50°$ for a uranium projectile one observes directly the onset of inelastic interactions at small impact parameters, resulting in a decrease of the observed ratio (Fig.

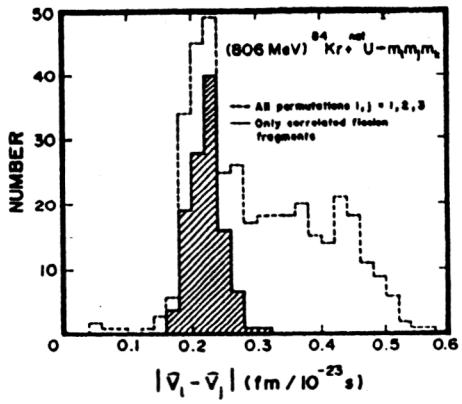

FIG. 18. Distribution of the Galilean invariant $v_{ij}=|v_i-v_j|$ for $i,j=1,2,3$ in the 3-particle exit channel for the reaction (806 MeV) ^{84}Kr+U. The histograms show all three possible combinations of correlated pairs (ij) together with the third particle (k). For each event we could find at least one combination of $(ij)k$ with (ij) in the range $v_{ij}=0.23\pm0.6$ fm/10^{-23} s (shaded area).[32]

17). The exact details of this decrease are obviously due to the special characteristics of the specific nuclear interaction.

It is of considerable interest to determine accurately the angle, called the quarter-point angle $\theta^{(1/4)}$, at which the experimental differential elastic scattering cross section is 1/4 of the elastic differential Rutherford cross section. On the basis of the model described in Ref. 98, one can correlate this experimental $\theta^{(1/4)}$ with the reaction parameter $R_{\rm int}$, the grazing angular momentum $l_{\rm gr}$, and the total reaction cross section σ_R.[102–106]

4.5. Evidence for sequential fission

4.5.1. Correlated fragment pairs and their characteristic velocities

Sequential interactions in nuclear reactions leading to more than two particles in the exit channel have significant resonances for certain kinematical variables.[107] Let us denote two outgoing particles by i and j, and their masses by m_i and m_j. A resonance in the Galilean invariant

$$v_{ij}^2=|\bar{v}_i-\bar{v}_j|^2 \tag{14}$$

at

$$v_{ij}=\mathring{v}_{ij} \tag{15}$$

describes a quasibound intermediate state whose decay energy E_{ij} is given by

$$E_{ij}=\frac{m_im_j}{2(m_i+m_j)}\,\mathring{v}_{ij}^2. \tag{16}$$

The resonance is well defined if the lifetime of the intermediate state is sufficiently long. The decay of the intermediate state can be influenced by other particles, resulting in the broadening of this resonance, in a shift of its position, and in nontrivial angular correlations of the outgoing products of the intermediate state.

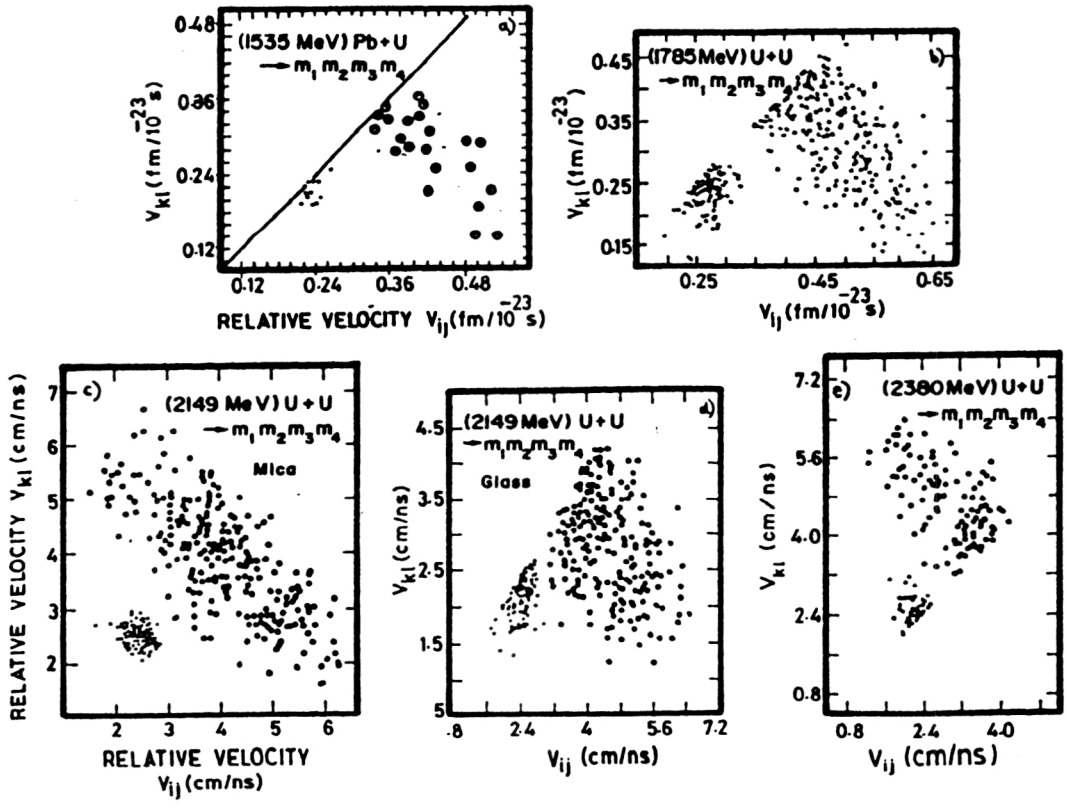

FIG. 19. Distribution of the Galilean invariant v_{ij} of two fragments against that of the complementary two fragments v_{kl} $(i,j,k,l=1,2,3,4)$ in the 4-particle exit channel for all three combinations. The results are shown on an event-by-event basis for five different studies (a–e).[21,33,45,56,58]

Typical distributions of the experimental velocity differences v_{ij} for reaction products in the three-particle and four-particle exit channels are shown in Figs. 18 and 19, respectively. Here we have integrated all the other variables. Figure 18 shows the velocity differences v_{ij}, for different combinations to couple the pair $[ij]$ with a third particle $[k]$ in the three-particle exit channel. Figure 19 shows the different possibilities to couple two pairs $[ij]$, $[kl]$ in the four-particle exit channel. Corresponding to the various combinatorial possibilities, we obtain three results for each event, displayed collectively in Fig. 18 for three-prong events and in Fig. 19 for four-prong events. For three-prong events we have pairs v_{ij}, v_{ik}, and v_{jk}. For four-prong events v_{ij} versus v_{kl}, v_{ik} versus v_{ji}, and v_{il} versus v_{jk} are plotted. In Figs. 18 and 19 one can observe a striking concentration of points near the following value of the relative velocity between two fragments:

$$v_{ij}=0.23 \text{ fm}/10^{-23} \text{ s}. \tag{17}$$

It is important to note that for each multiprong event one observed pairs of fragments with a velocity difference in the range

$$v_{ij}=(0.23\pm0.06) \text{ fm}/10^{-23} \text{ s}. \tag{18}$$

In four-prong events we could always find exactly one combination $[ij]$, $[kl]$ which fitted the condition of Eq. (18). This well-defined cluster can be seen in Fig. 19. The other combinations give a wide scatter of points clearly separated from this cluster.

For three-prong events one could find at least one combination $[ij]$, $[k]$ according to Eq. (18). Moreover, in about 80% of all cases we have one uniquely determined combination for $v_{ij}=0.23$ fm/10^{-23} s, while all other combinations differ significantly from this value. In about 20% of the events we could observe two different combinations, e.g., $[ij]$, $[k]$ and $[ik]$, $[j]$, which satisfied Eq. (18). Such a lack of uniqueness could also be observed if the two-dimensional representation was converted into a one-dimensional representation. The maximum is clearly observed for three-prong events at $v_{ij}=0.23$ fm/10^{-23} s, appearing significantly above the broad background distribution. Owing to this background, it is possible in 20% of all cases to find more than one combination according to Eq. (18).

The mean relative velocity observed in the fission of ^{235}U with thermal neutrons[108] has the value

$$v_{ij}=0.24 \text{ fm}/10^{-23} \text{ s}. \tag{19}$$

This value is nearly independent of the fragment mass ratio m_i/m_j between the fission fragments. It changes by 2% when going from symmetric to asymmetric fission. The natural dispersion in v_{ij} for a fixed mass ratio is 0.005 fm/10^{-23} s. The value of v_{ij} [Eq. (19)] is also nearly independent of the mass (m_{ij}) and charge (z_{ij}) of the fissioning fragment, and in particular (and surprisingly) independent of the excitation energy E_x. According to the literature,[92,108,109] the following values are to be expected:

$$v_{ij}=(0.24\pm0.04) \text{ fm}/10^{-23} \text{ s} \tag{20}$$

for 140 u$<m_{ij}<$300 u, 0 MeV$<E_x<$100 MeV, and $1.0<m_i/m_j<1.5$.

The analysis of velocity differences of various multifragment channels in all investigated heavy-ion reactions strongly indicates the sequential nature of the reaction mechanism. In the first step of a binary interaction, two excited ions are produced; one or both of these subsequently undergo fission in the second step of the reaction, resulting in three or four final fragments. In the case of five-prong events, one of the heavy fragments of the second step decays further sequentially. Denoting the projectile and target masses by m_P and m_T, respectively, the sequential nature of multifragment events is thus given as follows:

3-prong events: $m_P+m_T\rightarrow m_{ij}^*+m_k$ 1st step

m_i+m_j 2nd step

4-prong events: $m_P+m_T\rightarrow m_{ij}^*+m_{kl}^*$ 1st step

(m_i+m_j) (m_k+m_i) 2nd step

5-prong events:

$m_P+m_T\rightarrow m_{ij}^*+m_{klm}^*$ 1st step

(m_i+m_j) $(m_k+m_{lm}^*)$ 2nd step

(m_l+m_m) 3rd step

5-prong events:

The fission Q values of the intermediate fissioning nuclei agree well with the semi-empirical correlation of Viola.[109] The experimentally determined Q values deviate between $\pm$(4–25)% from those expected theoretically. The observation of correlations in the velocity difference v_{ij} between the reaction products could be confirmed by electronic methods for the three-particle exit channel in the reaction (1785 MeV) U+U and in some lighter reaction systems.[110,111] To our knowledge, the occurrence of multiple sequential fission in heavy-ion induced reactions leading to four or five heavy fragments in the exit channel has not been investigated so far by other methods.

4.5.2. Independence of the second reaction step for the sequential fission process

In the case of fast fission of a primary reaction product in the presence of the Coulomb field of a second binary reaction product, one would expect an anisotropic angular distribution in the scattering plane defined by vectors in the direction of motion of the two primary reaction products.[112] The in-plane angle is defined in Fig. 20. The investigation or analysis of the in-plane angular distribution of correlated fission fragments could reveal such effects. However, experimentally it was found that the in-plane angular distribution is isotropic within the moving c.m. system of the primary reaction products, as shown in Fig. 21 (top). The observed modulation in the experimental in-plane distribution is purely technical in nature and has no physical basis. This is

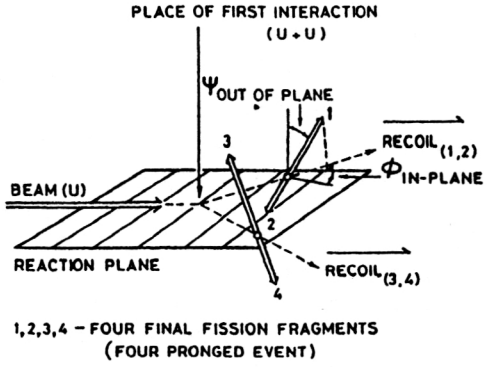

FIG. 20. Graphical description of the terms "reaction plane," "out-of-plane" angle, and "in-plane" angle.

due to the presence of fission fragments with flight directions parallel or perpendicular to the detector surface, which consequently remain undetected (see, e.g., Fig. 1). Our method is not accurate enough to allow a detailed study of the influence of the nuclear or Coulomb field of one primary reaction product on the fission configuration of the other primary reaction product.

The mass-ratio distribution m_i/m_j for fission fragments and the distribution of velocity differences are independent of the fission direction, as shown in Fig. 21 (rest). The out-of-plane angular distribution of fission fragments in the four-particle exit channel is shown in Fig. 22. (The definition of the out-of-plane angle is given in Fig. 20.) Obviously, there are no nontrivial correlations between the out-of-plane angles for both fission-fragment pairs. The distribution is consistent with the product of the two angular distributions. This gives an additional hint that the second reaction step is

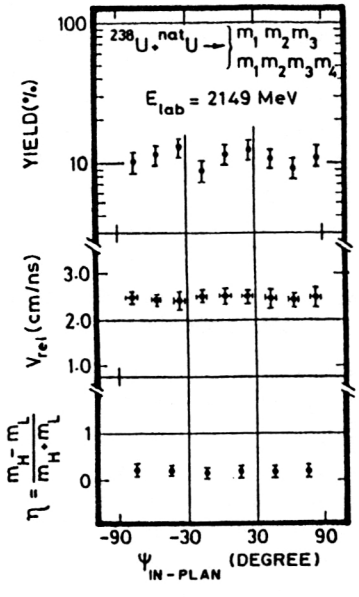

FIG. 21. Distribution of the yield for the "in-plane" angle, the relative velocity v_{ij} of correlated pairs of fission fragments, and of the asymmetry of the mass split in fission as a function of the "in-plane" angle for the reaction (2149 MeV) ^{238}U+U giving three or four particles in the exit channel. The "dips" in the yield at +60° and −30° are again due to technical reasons. Only statistical uncertainties are given.[58]

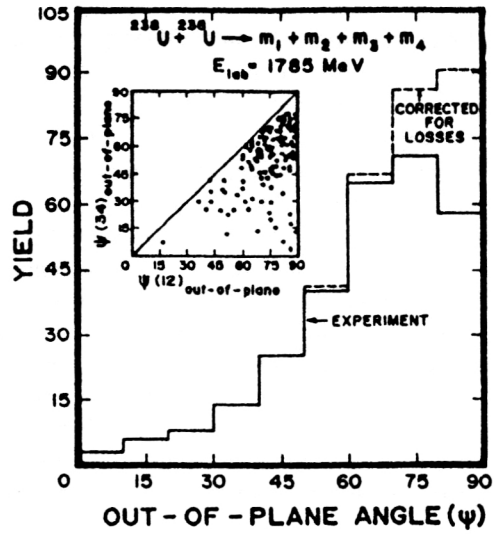

FIG. 22. Distribution of the "out-of-plane" angle (defined in Fig. 20) for fission fragments from the reaction (1785 MeV) ^{238}U+U→(4 particles) (outlined histogram). The dashed histogram gives a reconstructed (i.e., corrected) distribution, as the 2π geometry used is less sensitive in its registration efficiency for certain geometrical configurations.[48]

independent of the first reaction step. Nontrivial correlations for systems lighter than U+U have been observed. Here it was indeed observed that fission during the second reaction step still occurs in the presence of the first reaction partner.[33] However, these nontrivial correlations have also not been observed in the interaction (1785 MeV) ^{238}U+^{nat}U, using complex electronic counter systems.[110] This result from counter experiments is confirmed by the present work, based on the SSNTD technique for three and four particles in the exit channel for the interaction U+U up to energies of 2149 MeV (E_{lab}). At higher bombarding energies a complete analysis of the system U+U is still lacking.

4.6. The inelastic two-particle exit channel in the reaction (806 MeV) ^{84}Kr+^{nat}U

4.6.1. Energy and mass distribution

The total kinetic-energy loss (TKEL) in a nuclear reaction is defined as the difference of the kinetic energy in the exit channel and that in the entrance channel, both measured in the c.m. system. We define deep inelastic events as events with $|\text{TKEL}| \geq 120$ MeV. Most of the inelastic events have TKEL$\geq$250 MeV. We can calculate the Coulomb barrier for this reaction with R_{int}=14.0 fm to be E_{Coul}=340 MeV. For the interaction (806 MeV) ^{84}Kr+^{nat}U the c.m. energy is $E_{c.m.}$=596 MeV. By comparing these energies we notice that in deep inelastic two-particle events nearly complete damping has occurred for the available energy of the incoming ^{84}Kr ions. The kinetic energy of the fragments in the final channel is essentially determined by the mutual Coulomb repulsion. It is typical for these reactions that we occasionally observe even larger values for TKEL.[23]

Reaction products close to the projectile and target mass show nearly no energy loss. On the other hand, fragments due to deep inelastic interactions are coupled to greater mass transfer. This mass transfer goes from the heavy partner (ura-

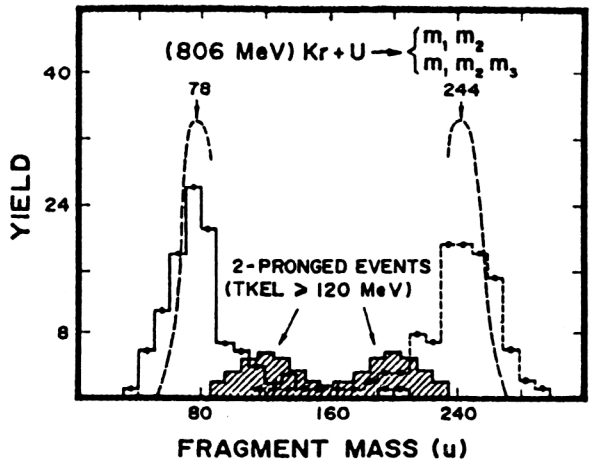

FIG. 23. Primary mass-yield curve of the first reaction step in the three-body exit channel for (806 MeV) ^{84}Kr+^{nat}U, integrated over angles and energies. Prefission fragments and surviving reaction products are denoted by open and full dots, respectively. The light dashed curves refer to the distributions after corrections for the experimental uncertainties ($\Delta m/m \approx 8\%$). Also displayed by the hatched histogram is the mass distribution of the deep inelastic component (TKEL$\geq$120 MeV) in the two-body channel (after corrections).[32]

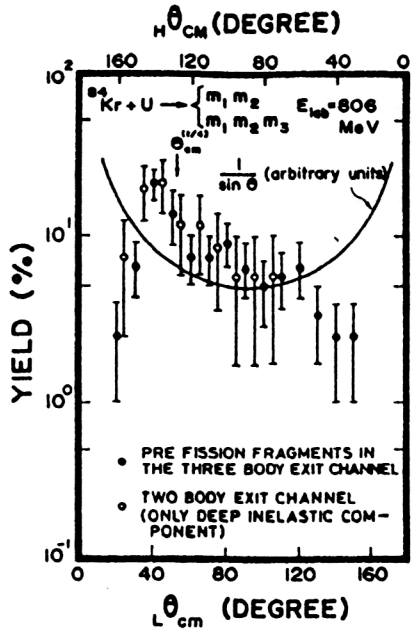

FIG. 24. Angular distribution in the c.m. system for deep inelastic products in the first interaction step of the reaction (806 MeV) ^{84}Kr+U, yielding two or three particles. In the 2-particle exit channel only events with TKEL$\geq$120 MeV have been included (deep inelastic component).

nium) to the light partner (krypton). The mass distribution of deep inelastic fragments has two maxima at $A=195$ and $A=118$, as shown in Fig. 23 (2-prong events). After correcting for experimental uncertainties, both peaks have widths of about 45 u (FWHM). For this correction we assumed the same experimental mass resolution in both the inelastic and elastic channels.

Radiochemical studies of the system Kr+U indicated a very strong maximum at $A=195$ ("Goldfinger"),[113] having a rather narrow width of only about 18 u (FWHM). This is contrary to the results of our work. Our peak is rather broad. Furthermore, this peak in the two-body channel resembles very much the mass distribution of heavy primary fragments (first reaction step) in the three-particle exit channel (e.g., Fig. 23). The heavy mass peak around $A=195$ in the two-body exit channel should thus be interpreted as being due to those primary fragments which, after a deep inelastic collision, survive subsequent decay. Therefore, a particular reaction mode which leads to "Goldfinger" need not be postulated. Furthermore, it is to be noted that we worked with a very precise and high Kr energy and that the above-mentioned radiochemistry work was done for lower energies down to the Coulomb barrier. Therefore this discrepancy will not be overemphasized. Additionally, the work by Lucas *et al.*,[114] based again on radiochemical techniques, indicated that the "Goldfinger" and its narrow distribution is an experimental artefact. Lucas *et al.* also used a very thin target (equivalent to a very well defined and high value of the ion energy) and determined the mass distribution of the binary reaction products. The maximum of higher mass in this distribution was near $A=195$, and its width was broad, as observed in our work. Lucas *et al.*[114] speculated that angular-momentum induced fission should produce predominantly fragments with $195<A<238$. For increasing angular momentum in the incoming reaction channel a shift of the maximum in the mass yield curve down to $A=195$ was expected. However, in view of our higher bombarding energies we should have expected a narrow mass distribution than in the results of Lucas *et al.*, who used a much lower bombarding energy. As we observe a rather broad experimental mass distribution, we cannot support the speculation of Ref. 114.

Another theoretical calculation based on a dynamical fragmentation model was carried out by Gupta[115] for the reaction ^{84}Kr+^{238}U. The collision process was described in a mass-asymmetry coordinate using the time-dependent Schrödinger equation. The Hamiltonian for the problem was constructed by making use of results derived from the classical orbit equations, the cranking model, and the BCS formalism. Gupta concluded that the Kr+U reaction at various energies is a peripheral collision with reaction times of the order of 6×10^{-21} s. Such reactions are characterized in general by low energy damping and only a few nucleon transfers. However, some specific partial waves in a narrow angular-momentum window allow for a considerable mass transfer and energy loss. The mass transfer was found to take place from the heavier to the lighter partner of the reaction.[115] Further, the cross section for the binary process is much smaller than for higher multiplicities. These results are in qualitative agreement with our experiments.

4.6.2. Angular distribution

The angular distribution in the c.m. system for deep inelastic 2-prong events is shown in Fig. 24 (open circles). This distribution was obtained after integrating over all the other variables. A strong decrease of projectile-like fragments at $\theta_{c.m.}<25°$ and for target-like recoils at $\theta_{c.m.}>155°$ is exclusively due to technical limitations of our 2π geometry. The distribution in Fig. 24 is weakly focused near the

quarter-point angle $\theta_{c.m}^{(1/4)}=47°$. We do not observe a strong decrease towards larger angles. We also find no sign of a $1/\sin(\theta_{c.m.})$ angular distribution. This shows that compound nuclear reactions play at best only a minor role. The reaction mechanism of multifragment breakup and subsequent fusion of two other fragments requires a definite maximum at forward and backward angles, as calculated in Ref. 25. The present experimental data do not indicate this feature. However, one should not overlook the fact that our 2π geometry is not well suited experimentally to study particularly these forward- and backward-peaked angular effects. In Fig. 24, it is seen that the deep inelastic two-prong events (open circles) and sequential fission (closed circles) show a very similar angular distribution.

The angular-distribution classification for heavy-ion reactions introduced by Galin[116] is based on a modified Sommerfeld parameter

$$\eta' = Z_P Z_T / h v', \tag{21}$$

where Z_P and Z_T are the electric charges of the projectile and target nucleus, respectively, and v' is the relative velocity between the target and the projectile at the peak of the interaction barrier. For low values of the parameter η' ($\eta'<200$) the angular distributions in the case of inelastic events are comparatively broad, with a maximum exceeding $\theta_{c.m.}^{(1/4)}$. For medium values of η' ($200<\eta'<250$), the angular distribution peaks in the forward direction and near the quarter-point angle with equal intensity. For higher values ($\eta'>250$) the differential cross section is strongly focused near the quarter-point angle. For the reaction (806 MeV) ^{84}Kr+^{nat}U we calculate the modified Sommerfeld parameter η' to be equal to 260. This value is similar to $\eta'=304$ for the reaction (686 MeV) ^{84}Kr+^{nat}U (Ref. 117). Therefore we observe in the two reactions rather similar angular distributions. In our experiment, the observed angular distribution and the focusing of the projectile-like fragments near the quarter-point angle strongly support the view that deep inelastic scattering takes place for grazing collisions with large mass transfer.[115]

4.7. Three-particle exit channel

4.7.1. Kinematical ambiguities

It has been mentioned earlier that in about 20% of all three-prong events the pair of fragments resulting from fission could not be uniquely identified in the case of reactions induced by uranium and lead ions on uranium target nuclei. The three-prong events observed in the interaction (806 MeV) ^{84}Kr+^{nat}U had an even higher contribution of about 35% of the events giving two possible pairs of fragments associated with sequential fission. This means that the track configurations allow two out of three possible combinatorial possibilities to group two fragments as a pair and a third particle as a spectator: (ij), k. The relative-velocity window $v_{ij}=0.23\pm0.06$ fm/10^{-23} s could be observed for two such combinations in each of the above-mentioned 20% of the three-prong events.

Whenever we observed only one kinematically acceptable solution, we observed predominantly forward scattering of projectile-like fragments and symmetric fission of the target-like heavy partner. This has to be expected, as we know that all excited nuclei or nuclei lighter than uranium fission predominantly symmetrically. Therefore, in the kinematical analysis of reactions induced by Kr and Pb ions we use the additional criterion that projectile-like fragments are scattered forward in the first reaction step whenever a nonunique situation arises with respect to the relative velocities.

For the reaction U+U this last-mentioned criterion cannot be applied. Here, in the case of nonuniqueness, we selected those combinations which provided the best agreement between the theoretical and empirical fission Q values.

4.7.2. Energy and mass distributions in the first reaction step

The energy and mass distribution was studied for several reactions using the present method of analysis. In the following, these reactions are discussed individually.

(1) (806 MeV) ^{84}Kr+^{nat}U.

The mass distribution in the first reaction step of the sequential process is shown in Fig. 23. The light component has its maximum at 78 u, while the peak of the heavy component is at 244 u. The heavy component of the first interaction step decays consecutively by sequential fission. After experimental corrections, one observes a narrow mass distribution having a width of 24 u (FWHM). As in the case of the inelastic two-particle exit channel, here too we observe a wide spectrum of Q values ranging from quasi-elastic interactions (TKEL$\approx$0 MeV) up to deep inelastic interactions.

This reaction is typical for heavy-ion reactions. The two-fragment exit channel is in principle very similar to the three-particle exit channel, the only new feature in the latter case being the sequential decay of its heavy reaction partner, particularly for the reaction partners with only small mass transfer.

(2) (1050 MeV) ^{84}Kr+^{nat}U.

As compared with the reaction (1) above, here the injection energy is increased from 256 to 436 MeV. The first-step masses were fitted in terms of Gaussian distributions, as shown in Fig. 25. The projectile-like mass is centered at 103 u, whereas the prefission mass distribution has its peak at 219 u. The reason for the enhanced central value of the projectile-like mass is discussed in detail in Ref. 35. Another difference observed here with respect to the reaction (1) is the increased widths of the mass distributions (e.g., from 24 u to 33 u for the projectile-like fragment).

(3) (1535 MeV) ^{208}Pb+^{nat}U.

The maxima in the mass distributions of the two components in the first reaction step are shifted towards greater asymmetry, as in (806 MeV) ^{84}Kr+^{nat}U. The light component has its maximum at about 200 u and does not undergo any further decay. The maximum of the heavy component is at about 250 u. These intermediate heavy nuclei decay in a second reaction step.

(4) (1785 MeV) ^{238}U+^{nat}U.

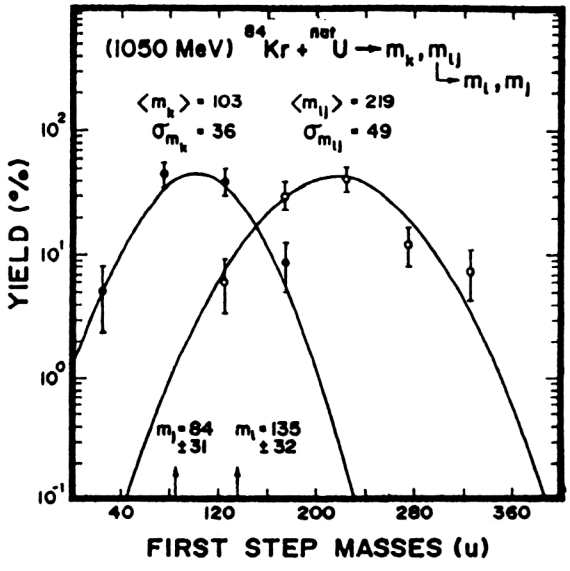

FIG. 25. Gaussian distributions for the projectile-like mass and the prefission mass in the first step of the three-body channel of the reaction $^{84}Kr+^{238}U$ at 12.5 MeV/u.[35]

In this case the distribution of both fragments in the first reaction step is symmetrical around $A=238$ u. The width of the distribution is 28 u, including experimental uncertainties. Unfolding this distribution into the surviving and decaying components, one obtains the following results: The mass distribution of the nonfissioning component (Fig. 26) has its maximum at 225 u, and its intensity decreases very steeply towards heavier masses. As we know from radiochemical data, one observes practically no nuclei with masses exceeding 238 in this reaction. Therefore the "surviving fragments" with masses $A>238$ u are artefacts due to our mass resolution of $\sigma=20$ u. The heavy prefission component peaks at 250 u. A slow decrease in the mass distribution of the heavy fragment indicates a considerable mass transfer in the first interaction step. This is a physically significant result. The system U+U was studied at 1785 MeV by several groups using the counter technique.[102,103] They found the centroid in the light and surviving component at $Z\simeq 86-88$. This agrees fairly well with our experimental value at $A=225$.

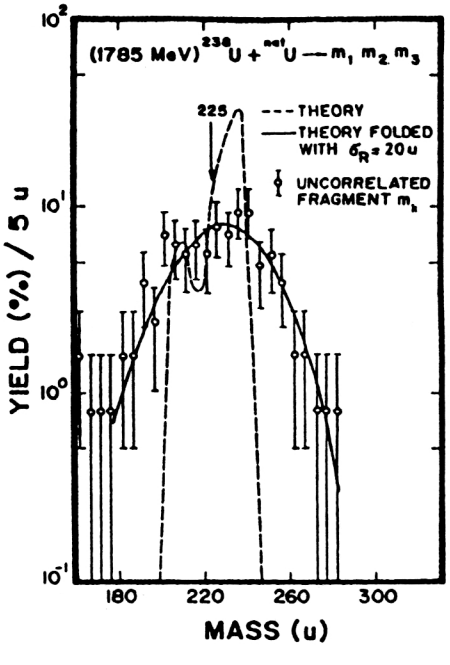

FIG. 26. Mass distribution of the surviving heavy transfer product in the reaction (1785 MeV) $^{238}U+U$ (3-particle exit channel). Only statistical uncertainties are given. The dashed curve is given according to diffusion calculations, including shell effects at $Z=82$, excitation energy $E_{ex}=75$ MeV, and interaction time $4\cdot 10^{-21}$ s.[118] The solid line is the same theoretical curve, but folded with an experimental uncertainty $\sigma=20$ u.

In Fig. 26 we also compare our experimental mass distribution with the one calculated theoretically.[118] The agreement is good. Furthermore, it agrees with radiochemical data.[119] We do not observe any shell effects in the mass distribution.

The reaction energy of the first step has its maximum at TKEL=0 MeV, indicating quasi-elastic scattering as the dominant process. This is rather surprising, as we have observed considerable mass transfer in the same interaction. However, several counter experiments confirm that in the interaction U+U, not too far from the Coulomb barrier, one observes comparably large mass transfers together with rather small energy dissipation.[102,111]

In summary, the reaction is quasi-elastic with considerable mass transfer, yielding a broad symmetric mass distribution in the first reaction step. All heavy partners with $A>238$ in the first interaction step decay in a second sequential fission step. The light fragments survive by about 50% (see also Table II).

(5) (2149 MeV) and (2380 MeV) $^{238}U+^{nat}U$.

The mass and energy distributions of the first interaction step in the 3-particle exit channel are rather similar at 1785, 2149, and 2380 MeV. However, we observe a larger energy dissipation at the higher bombarding energies. The intermediate mass distribution is always symmetrical around $A=238$, the surviving light component is always centered around $A=225$, and the intermediate heavy component is centered around $A=250$. The mass distribution of the intermediate masses is broader at 2149 MeV with $\sigma^{(3)}=31$ u, as compared with $\sigma^{(3)}=20$ u at 1785 MeV (Fig. 26). The same features can also be seen at $E_{lab}=2380$ MeV. Furthermore, at 2380 MeV, a quasi-elastic component with centroid at $A=238$ u and a broad shoulder towards lighter fragments can be observed, as far as the surviving fragments are concerned. With increasing energy dissipation, the asymmetry in the first reaction step is increasing.

The average total kinetic-energy loss ($\langle$TKEL$\rangle$) is 150 MeV and 184±55 MeV in (2149 MeV) $^{238}U+^{nat}U$ as measured with glass and mica detectors, respectively. Thus, the total kinetic-energy loss is significantly larger than for (1785 MeV) $^{238}U+^{nat}U$. The quoted value of $\langle$TKEL$\rangle$ is an average over all observed 3-prong events.

4.7.3. The distribution of scattering angle (c.m. system) in the first interaction step

(1) (806 MeV) $^{84}Kr+^{nat}U$.

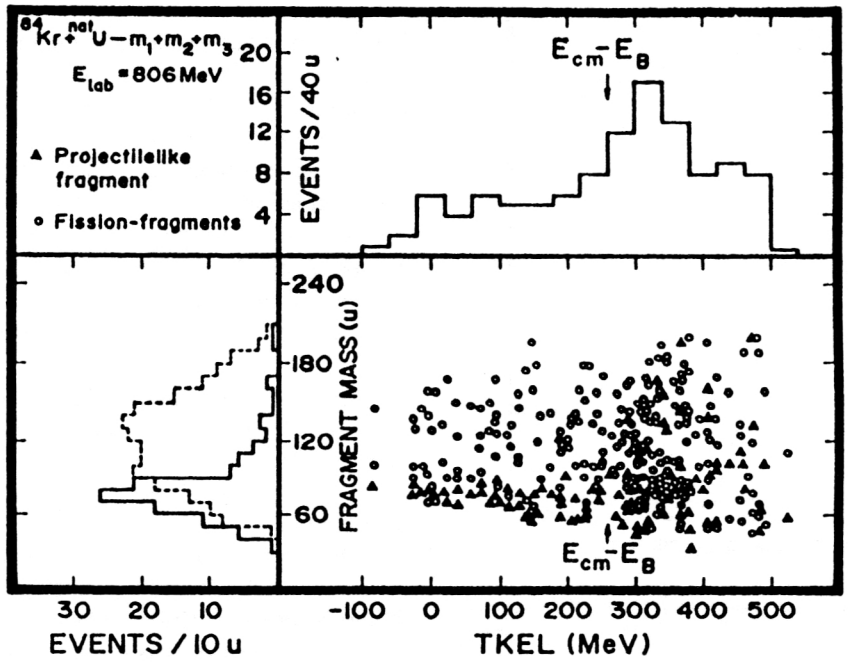

FIG. 27. Final mass distribution of the three-prong events in (806 MeV) $^{84}Kr+^{nat}U$, integrated over angles as a function of the total kinetic-energy loss (TKEL) in the first reaction step. Correlated fission-fragment pairs are shown by open points, and the uncorrelated spectator is indicated by the full triangle. No corrections due to experimental uncertainties have been employed.[32]

The angular distribution in the first reaction step for three-prong and inelastic two-prong events has been discussed earlier in Sec. 4.6.2. These angular distributions are rather similar in the two cases, as seen in Fig. 24. A peak near the quarter-point angle is strongly suggestive of a deep inelastic process.

(2) (1050 MeV) $^{84}Kr+^{nat}U$.

The analysis of two-prong events (elastic+quasi-elastic) yielded the value of the quarter-point angle as $\theta_{c.m.}^{(1/4)}=(33.5\pm0.5)°$. There was a significant fraction of three-prong events which involved a first-step scattering angle close to this value ($\theta_{lab}\sim24.9°$) and low TKEL. These events are clearly due to either a quasi-elastic or a deep inelastic process, since the initial asymmetry is almost preserved for the first reaction step. Events exhibiting the largest TKEL could be due to a quasifission type of reaction. Such events are characterized by a mass flow from the heavier to the lighter reaction partner and a scattering angle of the projectile-like fragment much greater than the quarter-point angle (for details, see Ref. 35).

(3) (1535 MeV) $^{208}Pb+^{nat}U$.

The angular distribution for the projectile-like reaction products of the first interaction step is concentrated around the quarter-point angle ($\Theta_{lab}^{(1/4)}=46°$), indicating the predominantly quasi-elastic character of this interaction.

(4) (1785 MeV and 2149 MeV) $^{238}U+^{nat}U$.

The distribution of scattering angles (c.m. system) for the two intermediate fragments produced in the 1785-MeV reaction is centered around 90°, as expected for such a symmetric system. The width of this distribution is 40° (FWHM). The absence of small or negative angles demonstrates the influence of the strong repulsive Coulomb force. A very similar angular distribution has been observed for the quasi-elastic events in a one-particle inclusive experiment using the counter technique in the same reaction at 1766 MeV.[120]

4.7.4. Mass distribution for individual fragments in the three-particle exit channel

(1) (806 MeV) $^{84}Kr+^{nat}U$.

For all 3-prong events of this reaction, a correlation plot of the individual final masses and their corresponding energies (TKEL) is shown in Fig. 27. Each event contributes three points on the scatter plot: the projectile-like fragment is shown as a filled triangle, whereas both fission fragments are plotted as open circles after integrating over all angles. The total kinetic-energy loss in the first interaction step shows a broad range of events originating from quasi-elastic to deep inelastic processes. Detailed investigations have shown that the mass drift as well as the width of the fission mass-yield curve increase with increasing energy dissipation. The fission-fragment mass-yield curve for events with large TKEL is centered around $A\simeq120$ u. For a very low TKEL, say, below 100 MeV, we observe an asymmetric fission-fragment mass-yield curve with maxima at 100 and 140 u, as known from the studies of low-energy fission.

(2) (1535 MeV) $^{208}Pb+^{nat}U$.

The distributions of individual masses in the three-particle exit channel of this reaction are similar to those shown in Fig. 27: one observes projectile-like fragments as well as light and heavy fission fragments, centered around

100 and 150 u. The asymmetric fission mass distribution indicates a low excitation energy of the intermediate system. This confirms the quasi-elastic nature of the first interaction step.

(3) (1785 MeV and 2149 MeV) ^{238}U+^{nat}U.

As stated in Sec. 4.7.2, the surviving light component is always centered around $A=225$ u, and the intermediate heavy component (which undergoes fission) peaks at $A=250$ u. At 1785 MeV, it can be seen from the mass-yield curve that the asymmetric character of the fission is still preserved. At the higher bombarding energy one can no longer see any obvious structure in the mass distribution of the final fragments. This mass-yield curve is symmetric around $A=125$ u. Unfolding this distribution into the light and heavy fission fragments, one obtains 105 and 145 u (glass detector, Ref. 46) and 97 and 153 u (mica detector, Ref. 58), respectively.

Altogether, the reaction U+U is characterized by an increasing inelasticity when the bombarding energy increases.

4.8. The four-particle exit channel

4.8.1. Energy and mass distribution in the first interaction step

(1) (806 MeV) ^{84}Kr+^{nat}U.

The first four-prong event ever found in heavy-ion interactions was observed in this reaction. Only one direct event was detected, and it was analyzed kinematically in detail. On the basis of this analysis, the reaction could be characterized as a sequential fission process with the first-step mass splitting given by

$$(84)+(238)\rightarrow(132\pm7)+(190\pm7);$$

$$\text{TKEL}=202\pm42 \text{ MeV}. \quad (22)$$

The quoted errors are based on the Monte Carlo simulation method discussed in Sec. 4.2.4. It is important to note that the intermediate fragments formed in the first reaction step involve a drastic mass transfer along with a considerable loss of energy. This shows that one can go from ^{238}U down to mass 190 (i.e., the Au nucleus) in such a reaction.

(2) (1050 MeV) ^{84}Kr+^{nat}U.

It is noticeable here that the first step again involved a large mass drift of 40–60 u towards symmetry and a kinetic-energy loss which is 50–80% of the entrance-channel c.m. energy, along with a scattering angle well above the quarter-point angle. These conditions strongly suggest the occurrence of a quasifission phenomenon in the first step of the reaction.

(3) (1535 MeV) ^{208}Pb+^{nat}U.

Here all four-prong events could be explained in terms of a sequential fission process. The mass distributions of the intermediate reaction products in the first interaction step are shown in Fig. 28. The light and heavy intermediate fragments have been unfolded. These are centered at $A=205$ u and $A=241$ u, respectively. The projectile-like and target-like intermediate fragments can be clearly distinguished. Statistically significant conclusions about mass drift or mass diffusion cannot, however, be drawn from our data.

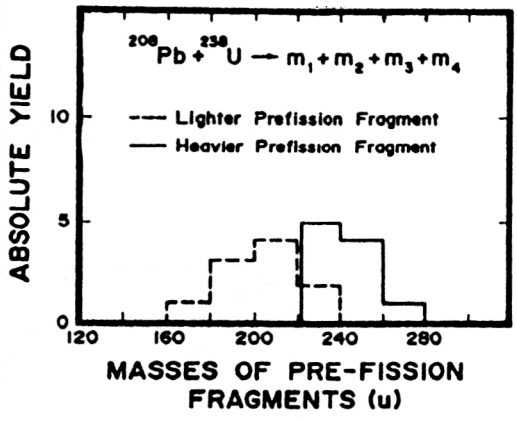

FIG. 28. Yield of first-step masses (without corrections for experimental uncertainties) in the case of the (1535 MeV) ^{208}Pb+^{nat}U reaction leading to four final masses, with separation of heavier and lighter first-step masses.[47]

The average energy loss in the first reaction step has been found to be $\langle\text{TKEL}\rangle=250$ MeV. The four-particle exit channel in (1535 MeV) ^{208}Pb+^{nat}U is thus characterized as a deep inelastic process, in contrast to the quasi-elastic character of the three-particle exit channel. This conclusion is statistically significant.

(4) (1785 MeV and 2149 MeV) ^{238}U+^{nat}U.

The mass distribution and the total kinetic-energy loss in the first interaction step at 1785 MeV exhibit no statistically significant difference between the 3-particle and the 4-particle exit channels. Both reaction channels are predominantly quasi-elastic. Obviously, the primary mass distribution is symmetrical around $A=238$ u.

Increasing the energy to 2149 MeV, the mass distribution in the first interaction step in the 4-particle exit channel becomes narrower than in the 3-particle exit channel.

As shown in Fig. 29, the ratio of the differential cross sections at 2149 MeV,

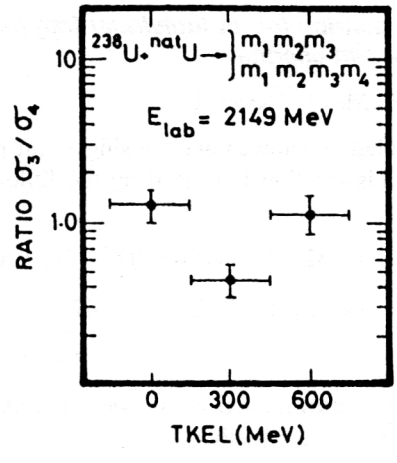

FIG. 29. Ratio of 3-prong events to 4-prong events within three intervals of TKEL losses: 0±150 MeV, 300±150 MeV, and 600±150 MeV. Only statistical uncertainties are given.[58]

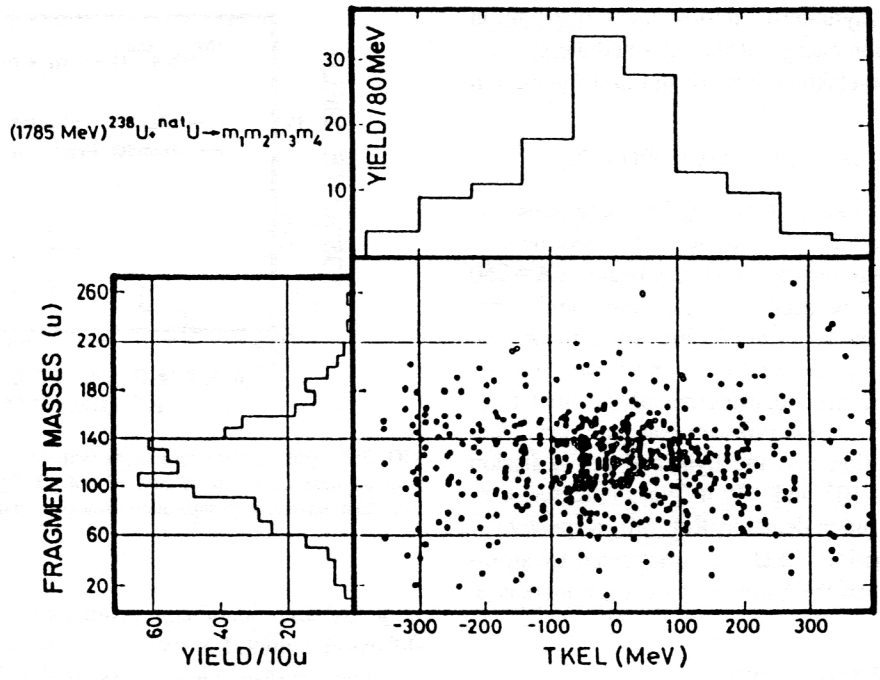

FIG. 30. Final fragment masses in the reaction (1785 MeV) ^{238}U+U as a function of the total kinetic-energy loss (TKEL) in the first interaction step. The results are uncorrected for uncertainties in the mass and energy determination.

$$\frac{d\sigma_3}{d\sigma_4}(\text{TKEL})=[d\sigma_3/d(\text{TKEL})]/[d\sigma_4/d(\text{TKEL})], \tag{23}$$

decreases at first with increasing total kinetic-energy loss. This was expected initially. However, for ever increasing TKEL we observe an increase in this ratio. Consequently, there are more 3-prong events than 4-prong events at the highest TKEL. This effect was first observed in Ref. 58. The interpretation of this observation could be as follows: In the three-particle exit channel of U+U one selects with increasing energy loss those intermediate products which are coupled to the largest mass transfer observed in this reaction. One of those intermediate products has become sufficiently light so as to become stable against subsequent fission.

4.8.2. Mass distribution of individual fragments in the four-particle exit channel

(1) (806 MeV) ^{84}Kr+^{nat}U.

Our calculations showed that the single four-prong event observed in this reaction is caused by the following decay chain:

^{84}Kr+^{nat}U→(132±7)*+(190±7)* 1st reaction step

(86±10), (46±15) (143±8), (47±7)

2nd reaction step.

The uncertainties quoted above were calculated by the Monte Carlo simulation method.

The experimental fission Q values of the intermediate fragments agreed fairly well with the empirical values expected from the Viola systematics[109] for ordinary fission, i.e.,

$$Q_{132}^{\text{exp}}=51\pm13 \text{ MeV}, \quad Q_{132}^{\text{emp}}=68 \text{ MeV}, \tag{24}$$

$$Q_{190}^{\text{exp}}=118\pm12 \text{ MeV}, \quad Q_{190}^{\text{emp}}=124 \text{ MeV}. \tag{25}$$

It is certainly premature to draw any definite conclusions from this single event. Nevertheless, it is interesting to note the rather asymmetrical mass split of the two intermediate products. It might be useful to recall that very light nuclei should split asymmetrically near the so-called Businaro–Gallone point.[121,122]

(2) (1785 MeV, 2149 MeV, and 2380 MeV)^{238}U+^{nat}U.

In Fig. 30 the correlation of the individual fragment masses and the total kinetic-energy loss in the first interaction step is shown event-by-event for 4-prong events observed at 1785 MeV. The data have not been corrected for experimental uncertainties. We observe a broad spectrum in TKEL, centered around TKEL=0 MeV. This indicates predominantly quasi-elastic interactions at 1785 MeV bombarding energy, resembling the quasi-elastic character of the reaction as seen in the 3-body channel. The resulting mass-yield curve shows an indication of an asymmetrical mass split. It resembles the well known mass-yield curve for the fission fragments of uranium at small excitation energies.

At the higher bombarding energy of 2149 MeV the resulting mass-yield curve is symmetrical. It is well centered around $A=120$ u, with a width of $\sigma_m=33$ u (corrected for experimental uncertainties). The distribution is similar to the one observed in the 3-particle exit channel.

At the even higher energy of 2380 MeV, we observe similar distributions, but with a lower statistical significance. The mass-yield curve is again centered around $A=120$ u, and the fission Q value is 169 MeV, just as expected for the fission of a uranium-like nucleus.

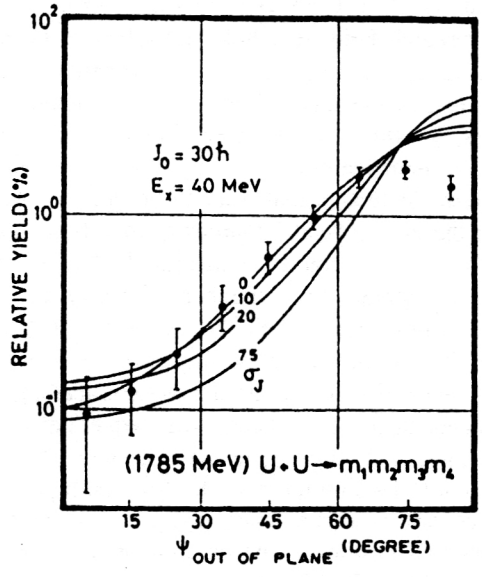

FIG. 31. "Out-of-plane" angular distribution of fission fragments for the reaction (1785 MeV) ^{238}U+U→(4 fragments), together with calculations based on the "charged-rotating-liquid-drop" model. The missing cross section for $\psi_{out}\sim 90°$ is due to technical reasons described in the text. The best fit could be obtained as follows: mean angular-momentum window $J=30\hbar$, mean excitation energy $E_x=40$ MeV, and angular-momentum window $\sigma_J\leq 10\hbar$. The calculations are based on the assumption of complete polarization ($J=M$).[21]

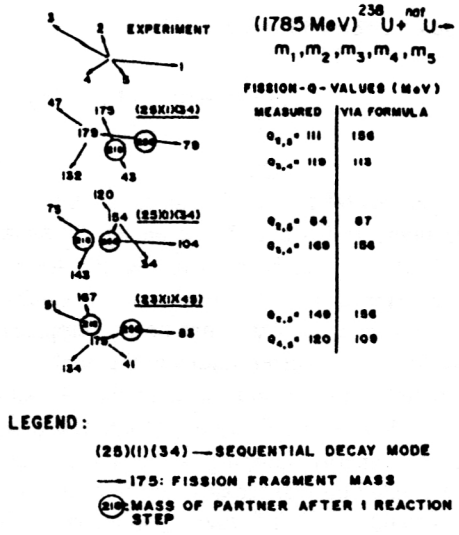

FIG. 32. Schematic representation of the trajectories of a five-prong event. Three combinational possibilities shown in the figure are consistent with a multiple sequential fission process.[48]

4.8.3. Angular distribution of fission fragments

In Fig. 31 the out-of-plane angular distribution of the final fragments in the 4-particle exit channel for the reaction (1785 MeV) ^{238}U+^{nat}U is shown (for the definition of the out-of-plane angle, see Fig. 20). The distribution of fission fragments is strongly focused within the "scattering plane" defined by the momentum vectors of the two reaction products after their first interaction step. Owing to our limited registration efficiency within the 2π-geometry SSNTD technique, we lose about 30% of all events, in particular close to $\psi_{out}\sim 90°$.

The lines drawn in Fig. 31 show the results of theoretical model calculations. Assuming completely polarized intermediate nuclei, we calculated the angular distribution as follows:

$$W(\psi_{out})=\sum_J \rho(J)\sum_{J=-K}^{+K}\rho(K)\{|D^J_{J,K}(\psi_{out})|^2 + |D^J_{J,-K}(\psi_{out})|^2\}, \quad (26)$$

where $\rho(J)$ and $\rho(K)$ are suitable distribution functions for the angular momentum J and its projection on the symmetry axis of the fissioning nucleus, and $D^J_{J,K}$ are the wave functions of a symmetrically deformed spinning top.

The model assumes symmetrically deformed fissioning nuclei. Furthermore, it is based on level densities, deformation parameters, and moments of inertia of an excited charged liquid drop rotating at the saddle-point deformation with all intrinsic degrees of freedom in thermal equilibrium. In the calculations we used a prefission mass $A=238$ and a level-density parameter $a=A/10$ (MeV^{-1}). Angular-momentum dependent equilibrium deformations, moments of inertia, and fission barriers were taken from Ref. 123.

The best fit to the experimental data was obtained with mean excitation energy of the fissioning nucleus $\langle E_x\rangle=40$ MeV and average angular momentum $\langle J\rangle=30\hbar$, having a width of $\sigma_J\leq 10\hbar$. This average angular momentum is somewhat lower than that calculated with the "sticking" model. For this sticking model the angular momentum can be estimated as $J=\frac{1}{7}l_{gr}=74\hbar$. The width of the K values obtained from the calculations varied between $10\hbar$ and $14\hbar$. This is of the same order of magnitude as the values previously used empirically for uranium-like nuclei.[92]

We obtained qualitatively the same results for the reactions (1535 MeV) Pb+U, (2149 MeV) U+U, and (2380 MeV) U+U. In each case, we observed a strong focusing of fission events within the reaction plane.

4.9. The 5-particle exit channel

This very rare decay process occurring in heavy-ion reactions can be studied with the SSNTD technique. So far, roughly two dozen 5-prong events have been observed in U+U interactions at different bombarding energies. Only two of these events have been completely analyzed, one at 1785 MeV and the other at 2149 MeV (see Table I). For the lower bombarding energy (1785 MeV) we obtained three different sets of physically reasonable solutions, as shown in Fig. 32. All solutions are compatible with a multiple sequential decay process taking place in three distinct reaction steps. The solution with the best agreement between the experimental and the Viola-type fission Q-value systematics[109] is as follows:

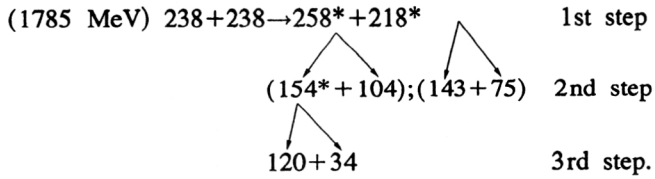

The experimental fission Q values of the intermediate reaction products 154 u and 218 u are $Q_{154}=84$ MeV and $Q_{218}=169$ MeV. As can be seen in Fig. 32, the agreement between the experimental and empirical Q values is quite remarkable. However, this will not be overemphasized. We determined the relative uncertainties in the nuclear masses to be approximately ± 15 u and those in the Q values to be $\Delta E/E=20\%$. Here we used again a Monte Carlo simulation calculation. The energy damping in the first interaction step could be calculated only approximately, owing to the experimental uncertainties in the track parameters: TKEL(first step)$=200\pm 100$ MeV. This indicates that the relative kinetic energy in the entrance channel, $E_{\text{c.m.}}-E_{\text{Coul}}=165$ MeV, has been almost completely damped in this interaction.

The analysis of the 5-prong event observed at 2149 MeV confirms the sequential reaction mechanism. This event could be analyzed as follows:

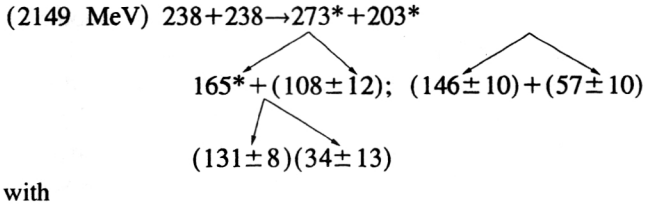

with

$$Q_{203}^{\text{exp}}=(127\pm 18)\ \text{MeV} \quad \text{and} \quad Q_{203}^{\text{emp}}=138\ \text{MeV},$$

$$Q_{165}^{\text{exp}}=(84\pm 26)\ \text{MeV} \quad \text{and} \quad Q_{165}^{\text{emp}}=98\ \text{MeV}.$$

Here TKEL(first step)$=490\pm 60$ MeV, which is to be compared with $(E_{\text{c.m.}}-E_{\text{Coul}})=250$ MeV.

Both 5-prong events are thus attributable to the multiple sequential fission process, where in the first interaction step two excited primary fragments are formed as a result of a binary deep inelastic interaction. The first step is characterized by complete energy damping and considerable mass transfer (~20–30 u). In the second step the lighter of the two primary fragments undergoes subsequent single fission, whereas the heavier fragment fissions sequentially in steps 2 and 3.

The mass asymmetry is remarkable. The asymmetry value has been determined for both events and seems to increase with increasing sequential reaction steps:

$$(1785\ \text{MeV}):\ \eta(258)=0.194,\quad \eta(218)=0.312,\quad \eta(154)=0.558;$$

$$(2149\ \text{MeV}):\ \eta(273)=0.216,\quad \eta(203)=0.438,\quad \eta(166)=0.590.$$

5. CONCLUSION

The investigation of heavy-ion induced nuclear reactions with high multiplicity in the exit channel using the SSNTD (Solid State Nuclear Track Detectors) has opened up an interesting research field. A simple and effective method has been introduced to extract from the experimentally observed track parameters the inherent physical parameters, such as the masses, Q values, and energies. This method is basically exclusive. Kinematically complete spectroscopic information on the intermediate and final reaction products could be obtained for the 2-, 3-, 4-, and 5-prong events. In addition, the reaction mechanism could be identified. The kinematical analysis was applied to a number of heavy-ion induced nuclear reactions, mostly with $^{\text{nat}}$U as the target. Using this technique, it was shown for the first time by direct experimental evidence that heavy-ion interactions leading to 3, 4, or 5 particles in the exit channel are sequential in nature. From the measured lengths and the directions of correlated tracks, it could be inferred that the high-multiplicity reactions are consistent with a binary first reaction step followed by a sequential fission of one or both of the two primary reactions products. Within our experimental uncertainty, no final-state interactions between the fragments could be determined, i.e., all our data are consistent with a reaction pattern where the primary products escape from the range of their initial nuclear interaction prior to a decay via a sequential fission process. This interpretation has been confirmed with other experimental techniques and is now generally accepted.

The authors want to thank the staff of the LINAC in Manchester and the UNILAC in Darmstadt for kindly arranging the irradiations with heavy ions. Stimulating discussions with many colleagues are acknowledged. The help of Dr. K. Rashid (ICCC, Islamabad) in preparing earlier versions of this manuscript is gratefully appreciated. We have to thank the Pakistan Atomic Energy Commission (PAEC, Islamabad), in particular Dr. Ishfaq Ahmad, Chairman, PAEC and Dr. N. A. Khan and Dr. I. H. Qureshi, former Directors of PINSTECH (Islamabad), the International Office of the Kernforschungs-Zentrum Karlsruhe (KfK, Karlsruhe), the Deutscher Akademischer Austauschdienst (DAAD, Bonn), and the Alexander-von-Humboldt Foundation (Bonn) for making possible mutual working visits in Pakistan and Germany. This work was supported in part by the PAEC (Islamabad), the BMFT (Bonn), the DFG (Bonn), the GSI (Darmstadt), the IAEA (Vienna), and others.

[1)] Visiting Scientist.

[1] D. A. Young, Nature **182**, 375 (1958).
[2] E. C. H. Silk and R. S. Barnes, Phil. Mag. **4**, 970 (1959).
[3] P. B. Price and R. M. Walker, J. Appl. Phys. **33**, 2625 (1962).
[4] R. L. Fleischer, P. B. Price, and R. M. Walker, Ann. Rev. Nucl. Sci. **15**, 1 (1965).
[5] R. L. Fleischer, P. B. Price, and R. M. Walker, *Nuclear Tracks in Solids* (University of California Press, Berkeley, 1975).
[6] S. A. Durrani and R. K. Bull, *Solid State Nuclear Track Detection* (Pergamon Press, Oxford, 1987).
[7] R. Spohr, *Ion Tracks and Microtechnology* (Vieweg, Germany, 1990).
[8] *Nucl. Tracks Radiat. Meas.*, Special Volumes No. 8 (1984), No. 12 (1986), No. 15 (1988), and No. 19 (1990). References to earlier conferences therein.
[9] *Treatise on Heavy-Ion Science*, edited by D. A. Bromley (Plenum Press, New York, 1984).

[10]P. B. Price, R. L. Fleischer, R. M. Walker, and E. L. Hubbard, in *Proc. of the Third Conf. on Reactions Between Complex Nuclei*, Asimolar (University of California Press, Berkeley, 1963).
[11]R. L. Fleischer, P. B. Price, R. M. Walker, and E. L. Hubbard, Phys. Rev. **143**, 943 (1966).
[12]V. P. Perelygin, N. H. Shadieva, S. P. Tretiakova, A. H. Boos, and R. Brandt, Nucl. Phys. **A127**, 577 (1969).
[13]P. Vater and R. Brandt, Radiochim. Acta **21**, 191 (1974).
[14]P. Vater, H. J. Becker, and R. Brandt, J. Radioanal. Chem. **32**, 275 (1976).
[15]P. Vater, H. J. Becker, and R. Brandt, Nucl. Instrum. Methods **147**, 271 (1977).
[16]G. Fiedler, R. Haag, J. Aschenbach, and T. Rautenberg, Gesellschaft für Schwerionenforschung, Darmstadt Report GSI-J-1-77 (1977), p. 131.
[17]G. Fiedler, J. Aschenbach, W. Otto, T. Rautenberg, U. Steinhauser, and G. Siegert, Nucl. Instrum. Methods **147**, 35 (1979).
[18]B. Grabez, Z. Todorovic, and R. Antanasijevic, in *Proc. of the 10th Intern. Conf. on SSNTD*, Lyon, 1979 (Pergamon Press, 1980), p. 899.
[19]M. Debeauvais, S. Jokic, and J. Tripier, in *Proc. of the 10th Intern. Conf. on SSNTD*, Lyon, 1979 (Pergamon Press, 1980), p. 927.
[20]P. Vater, H. J. Becker, R. Brandt, and H. Freiesleben, Phys. Rev. Lett. **39**, 594 (1977).
[21]P. A. Gottschalk, P. Vater, H. J. Becker, R. Brandt, G. Grawert, G. Fiedler, R. Haag, and T. Rautenberg, Phys. Rev. Lett. **42**, 359 (1979).
[22]M. Debeauvais, J. Ralarosy, J. Tripier, and S. Jokic, Nucl. Tracks **8**, 515 (1984).
[23]W. U. Schroeder, J. R. Huizenga, in *Treatise on Heavy-Ion Science*, edited by D. A. Bromley, Vol. 2 (Plenum Press, New York, 1984), p. 115.
[24]S. A. Karamyan, Yu. Ts. Oganessian, B. I. Pustylnik, and G. N. Flerov, in *Physics and Chemistry of Fission* (IAEA, Vienna, 1969), p. 759.
[25]H. H. Deubler and K. Dietrich, Phys. Lett. **62B**, 369 (1976).
[26]H. Backe, F. Weik, P. A. Butler, V. Metag, J. B. Wilhelmy, D. Habs, G. Himmele, and H. J. Specht, Phys. Rev. Lett. **43**, 1077 (1979).
[27]P. Vater, Dissertation, Marburg (1976).
[28]M. Ait-Salem *et al.*, Nucl. Instrum. Methods **60**, 45 (1968).
[29]G. Remy *et al.*, J. Phys. **31**, 27 (1970).
[30]M. Debeauvais and J. Tripier, Nucl. Instrum. Methods **173**, 157 (1980).
[31]J. Tripier *et al.*, Nucl. Instrum. Methods **115**, 29 (1974).
[32]P. A. Gottschalk, G. Grawert, P. Vater, and R. Brandt, Phys. Rev. C **27**, 2703 (1983).
[33]R. Haag, G. Fiedler, R. Ulbrich, G. Breitbach, and P. A. Gottschalk, Z. Phys. A **316**, 183 (1984).
[34]P. Vater *et al.*, Nucl. Tracks Radiat. Meas. **11**, 5 (1986).
[35]I. E. Qureshi *et al.*, Nucl. Phys. **A477**, 510 (1988); Phys. Rev. C **37**, 393 (1988).
[36]R. Bougault *et al.*, Nucl. Instrum. Methods A **259**, 473 (1987).
[37]G. Rudolf *et al.*, Nucl. Instrum. Methods A **307**, 325 (1991).
[38]M. M. Fowler *et al.*, Nucl. Instrum. Methods A **281**, 517 (1989).
[39]D. Drain *et al.*, Nucl. Instrum. Methods A **281**, 528 (1989).
[40]J. Andrew *et al.*, Phys. Rev. C **45**, 2423 (1992).
[41]M. T. Magda *et al.*, Phys. Rev. C **45**, 1209 (1992).
[42]M. Begemann-Blaich *et al.*, Phys. Rev. C **45**, 677 (1992).
[43]L. Stuttge *et al.*, Nucl. Phys. **A539**, 511 (1992).
[44]H. A. Khan *et al.*, Kerntechnik **49**, 236 (1987).
[45]G. Breitbach, Diplomarbeit, Justus Liebig Universität, Giessen (1983).
[46]R. Haag, Dissertation, Justus Liebig Universität, Giessen (1981).
[47]T. Rautenberg, Diplomarbeit, Justus Liebig Universität, Giessen (1980).
[48]R. Brandt, P. A. Gottschalk, and P. Vater, Nucl. Instrum. Methods **173**, 111 (1980).
[49]H. A. Khan, K. Rashid, R. Akbar, G. Hussain, P. Vater, P. A. Gottschalk, and R. Brandt, Nucl. Instrum. Methods **173**, 155 (1980).
[50]G. Fiedler, P. A. Gottschalk, P. Vater, R. Brandt, G. Grawert, R. Haag, and T. Rautenberg, in *Proc. of the Symp. on Physics and Chemistry of Fission*, Juelich, 1979 (IAEA, Vienna).
[51]R. Haag, G. Fiedler, T. Rautenberg, P. A. Gottschalk, and G. Grawert, in *Proc. of the 10th Intern. Conf. on SSNTD*, Lyon, 1979 (Suppl. 2 to Nucl. Tracks, 1980), p. 933.
[52]R. Brandt, P. Vater, B. Grabez, and P. A. Gottschalk, in *Proc. of the Intern. Conf. on Nuclear Physics* [LBL (1980); LBL-11118 (1980), p. 481].
[53]H. A. Khan, R. Beckmann, P. Vater, P. A. Gottschalk, R. Brandt, and K. Jamil, in *Proc. of the 11th Intern. Conf. on SSNTD*, Bristol, 1981 (Suppl. 3 to Nucl. Tracks, 1982), p. 775.
[54]G. Fiedler, R. Haag, P. Crombach, G. Breitbach, P. A. Gottschalk, P. Vater, E. U. Khan, R. Beckmann, and R. Brandt, in *Proc. of the 11th Intern. Conf. on SSNTD*, Bristol, 1981 (Suppl. 3 to Nucl. Tracks, 1982), p. 779.
[55]H. A. Khan, I. E. Qureshi, W. Westmeier, R. Brandt, and P. A. Gottschalk, Phys. Rev. **32**, 1551 (1985).
[56]G. Fiedler, U. Steinhauser, T. Rautenberg, R. Haag, and P. A. Gottschalk, Nucl. Instrum. Methods **173**, 85 (1980).
[57]H. A. Khan, G. Tress, P. Vater, and R. Brandt, Nucl. Tracks **4**, 109 (1980).
[58]E. U. Khan, Dissertation, Philipps Universität, Marburg (1985).
[59]M. Zamani, J. Ralarosy, and M. Debeauvais, Nucl. Tracks Radiat. Meas. **12**, 321 (1986).
[60]H. A. Khan *et al.*, Nucl. Tracks Radiat. Meas. **12**, 341 (1986).
[61]H. Afarideh, *et al.*, Nucl. Tracks Radiat. Meas. **15**, 441 (1988).
[62]I. E. Qureshi *et al.*, Nucl. Tracks Radiat. Meas. **15**, 457 (1988).
[63]M. Ahmad *et al.*, Nucl. Tracks Radiat. Meas. **15**, 453 (1988).
[64]H. A. Khan *et al.*, Nucl. Tracks Radiat. Meas. **15**, 449 (1988).
[65]R. L. Fleischer, P. B. Price, R. M. Walker, and E. L. Hubbard, Phys. Rev. **156**, 353 (1967).
[66]J. Lindhard, M. Scharff, H. E. Schiott, K. Dan. Vidensk. Selsk. Mat.-Fys. Medd. **33**, (1963).
[67]N. Bohr, K. Dan. Vidensk. Selsk. Mat.-Fys. Medd. **18**, (1948).
[68]G. Tress, Diplomarbeit, Philipps Universität, Marburg (1978).
[69]L. C. Northcliffe and A. Schilling, Ann. Rev. Nucl. Sci. **13**, 67 (1963); Nucl. Data Tables A **7**, 233 (1970).
[70]H. Blok, F. M. Kiely, and B. D. Pate, Nucl. Instrum. Methods **100**, 403 (1972).
[71]J. B. Natowitz, A. Khodai-Joopari, J. M. Alexander, and T. D. Thomas, Phys. Rev. **169**, 993 (1968).
[72]H. H. Heckman, B. L. Perkins, W. G. Simon, F. M. Smith, and W. H. Barkas, Phys. Rev. **117**, 544 (1960).
[73]J. M. Alexander and M. F. Gazdik, Phys. Rev. **120**, 874 (1960).
[74]J. B. Niday, Phys. Rev. **121**, 1471 (1961).
[75]V. E. Noshkin, Jr. and T. T. Sugihara, J. Inorg. Nucl. Chem. **27**, 943, 959 (1965).
[76]T. H. Ormrod and H. E. Duckworth, Can. J. Phys. **41**, 1424 (1963).
[77]J. H. Ormrod, G. R. MacDonald, and H. E. Duckworth, Can. J. Phys. **43**, 275 (1965).
[78]B. Fastrup, P. Hvelplund, and C. A. Sautter, K. Dan. Vidensk. Selsk. Mat.-Fys. Medd. **35**, 10 (1966).
[79]J. A. Davies, L. Eriksson, and P. Jespersgaard, Nucl. Instrum. Methods **38**, 245 (1965).
[80]K. H. Schmidt, H. Wohlfarth, H. G. Clerc, W. Lang, H. Schrader, and K. E. Pferdekämper, Nucl. Instrum. Methods **134**, 157 (1976).
[81]B. Tamain, R. Chechik, H. Fuchs, F. Hanappe, M. Morjean, C. Ngo, J. Peter, M. Dakowski, B. Lucas, C. Mazur, M. Ribrag, and C. Signarbieux, Nucl. Phys. **A330**, 253 (1979).
[82]J. Terrell, Phys. Rev. **127**, 880 (1962).
[83]P. A. Gottschalk, P. Vater, H. J. Becker, R. Brandt, G. Grawert, G. Fiedler, R. Haag, and T. Rautenberg, in *Intern. Workshop on Gross Properties of Nuclei and Nuclear Excitations IV* (Hirschegg, Kleinwalsertal, 1978), AED-Conf 78-007-28.
[84]A. A. Saxena, K. K. Dwivedi, and G. Fiedler, Nucl. Tracks Radiat. Meas. **15**, 327 (1988).
[85]S. Ghosh, A. Saxena, and K. K. Dwivedi, Radiat. Eff. Defects Solids **112**, 149 (1990).
[86]K. K. Dwivedi, Nucl. Tracks Radiat. Meas. **19**, 71 (1991).
[87]E. V. Benton and R. P. Henke, Nucl. Instrum. Methods **67**, 87 (1969).
[88]S. Mukherji and B. K. Srivastava, Phys. Rev. **9**, B3708 (1974).
[89]F. Hubert *et al.*, Suppl. Aux. Ann. Phys. (Paris) **5**, 1 (1980).
[90]E.g., see: C. A. Sautter and E. J. Zimmermann, Phys. Rev. **140**, A490 (1965).
[91]E.g., see: F. Nickel, D. Marx, K. Guttner, S. Hofmann, and G. Muenzenberger, Z. Phys. A **288**, 125 (1978).
[92]R. Vandenbosch and J. R. Huizenga, *Nuclear Fission* (Academic Press, New York, 1973).
[93]F. M. Kiely and B. D. Pate, Nucl. Instrum. Methods **109**, 355 (1973).
[94]C. D. Milton and J. S. Fraser, Can. J. Phys. **40**, 1626 (1962).
[95]N. K. Aras, M. P. Menou, and G. E. Gordon, Nucl. Phys. **69**, 337 (1965).
[96]H. A. Khan *et al.* Nucl. Instrum. Methods B **28**, 41 (1987).
[97]W. E. Frahn, Ann. Phys. (N.Y.) **72**, 524 (1972); Nucl. Phys. **A302**, 267 (1978).
[98]J. S. Blair, Phys. Rev. **95**, 1218 (1954).
[99]T. D. Thomas, Phys. Rev. **116**, 703 (1959).

[100]W. D. Myers, Nucl. Phys. **A204**, 465 (1973).
[101]J. Blocki, J. Randrup, W. J. Swiatecki, and C. F. Tsang, Ann. Phys. (N.Y.) **105**, 427 (1977).
[102]J. R. Birkelund, J. R. Huizenga, H. Freiesleben, K. L. Wolf, J. P. Unik, and V. E. Viola, Jr., Phys. Rev. C **13**, 133 (1976).
[103]K. D. Hildenbrand, H. Freiesleben, F. Pühlhofer, W. F. W. Schneider, R. Bock, D. V. Harrach, and H. J. Specht, Phys. Rev. Lett. **39**, 1065 (1977).
[104]W. E. Frahn, Nucl. Phys. **A302**, 301 (1978).
[105]J. A. McIntyre, K. H. Wang, and L. C. Becker, Phys. Rev. **117**, 1337 (1960).
[106]R. A. Broglia and A. Winther, *Heavy Ion Reactions*, Vol. 1 (*Elastic and Inelastic Reactions*) (Benjamin-Cummings, London, 1981).
[107]C. Zupancic, Rev. Mod. Phys. **37**, 330 (1965).
[108]F. Hanappe, C. Ngo, J. Peter, and B. Tamain, in *Proc. of the IAEA Symposium on Physics and Chemistry of Fission*, Rochester, N.Y., 1973, Vol. 11, p. 289.
[109]V. E. Viola, Jr., Nucl. Data Sect. A **1**, 391 (1966).
[110]P. Glässel, D. V. Harrach, Y. Civelekoglu, R. Männer, H. J. Specht, J. B. Wilhelmy, H. Freiesleben, and K. D. Kildenbrand, Phys. Rev. Lett. **43**, 1483 (1979).
[111]D. V. Harrach, P. Glässel, Y. Cievelekoglu, R. Männer, and H. J. Specht, Phys. Rev. Lett. **42**, 1728 (1979).
[112]H. Kroeger and W. Scheid, Nucl. Phys. **A346**, 216 (1980).
[113]J. V. Kratz, A. E. Norris, and G. T. Seaborg, Phys. Rev. Lett. **33**, 502 (1974).
[114]R. Lucas, J. Poitou, J. V. Kratz, and G. Wirth, Z. Phys. A **290**, 327 (1979).
[115]R. K. Gupta, Phys. Rev. C **21**, 1278 (1980).
[116]J. Galin, in *Proc. of the European Conference on Physics with Heavy Ions*, Can. J. Phys. Suppl. C **5**, 83 (1976).
[117]R. J. Otto, G. T. Seaborg, and M. M. Fowler, Phys. Rev. C **17**, 1071 (1978).
[118]B. Schürmann *et al.*, Z. Phys. A **286**, 263 (1978).
[119]M. Schaedel, J. V. Kratz, H. Ahrens, W. Bruechle, G. Frauz, H. Gäggeler, I. Warnecke, G. Wirth, G. Herrmann, N. Trautmann, and M. Weis, Phys. Rev. Lett. **41**, 469 (1978).
[120]H. Freiesleben, K. D. Hildenbrand, F. Pühlhofer, W. F. W. Schneider, and R. Bock, Z. Phys. A **292**, 171 (1979).
[121]U. L. Businaro and Z. Gallone, Nuovo Cimento **1**, 629, 1277 (1955).
[122]J. R. Nix, Nucl. Phys. **A130**, 241 (1969).
[123]S. Cohen, F. Plasil, and W. J. Swiatecki, Ann. Phys. (N.Y.) **82**, 557 (1974).

This article was published in English in the original Russian journal. It is reproduced here with the stylistic changes by the Translation Editor.